AN EXPERIMENTAL AND THEORETICAL STUDY

OF THE

FLOW FIELD SURROUNDING A SUCTION PIPE INLET

By

William J. Apgar and David R. Basco
Coastal, Hydraulic, and Ocean Engineering Group
Civil Engineering Department
Texas A&M University

October 1973

TAMU-SG-74-203

Partially supported through Institutional Grant 04-3-158-18
to Texas A&M University
by the National Oceanic and Atmospheric
Administration's Office of Sea Grants
Department of Commerce

Center for Dredging Studies
Report No. 172

$3.00

Order from:

Department of Marine Resources Information
Center for Marine Resources
Texas A&M University
College Station, Texas 77843

ABSTRACT

The object of the present study was to develop a mathematical model of the flow field around a single suction pipe inlet near a horizontal boundary in an infinite reservoir. The basis for the theoretical approach was potential flow theory which neglects frictional and viscous effects. For simplicity, a point sink was employed. In order to investigate the actual flow conditions, an experimental apparatus was developed to test a model suction inlet. The inlet was a simple cylindrical pipe placed at various heights from and at an angle to the horizontal boundary.

The experimental results did conform to the theoretical for initial flow conditions when viscous effects were small. The viscous effects subsequently caused an altered flow with zones of separation. The resulting flow development negated the value of the potential flow solution.

PREFACE

A complete outline of a research program to evaluate and improve the performance of hydraulic dredge cutterhead systems has been described elsewhere by Basco and Dominguez*. The work described herein is only the first, preliminary step under flow conditions which are greatly simplified at the suction inlet.

The report was primarily written by the first author listed in partial fulfillment of the Master of Science requirement under the supervision of the second author listed who was the major advisor.

Special thanks are due to those who assisted in the construction of the experimental facility: Geral Greer, Won Oh Song, Jack Dysart, and Paul Versowsky; to Randy Long for reducing the photographic data; and to Mark Puckett for programming the flow equations.

The study was sponsored by the Center for Dredging Studies at Texas A&M University. The support of those industries making financial contributions to the Center is gratefully appreciated. Publication of this report was made possible through the Texas A&M University Sea Grant College Program.

*Basco, D. R. and Dominguez, R. F., "A Cutterhead Evaluation and Improvement Program", Proceedings, WODCON IV, World Dredging Conference, New Orleans, Dec. 1971, p. 561-

TABLE OF CONTENTS

LIST OF FIGURES

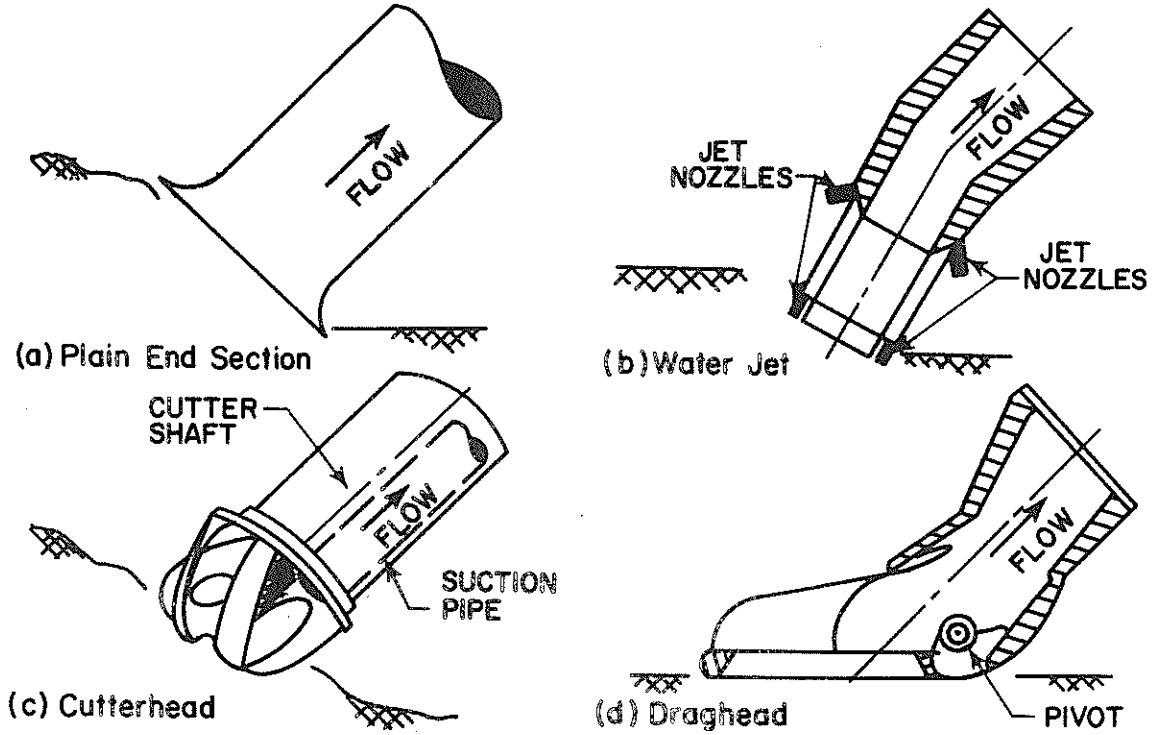

Types of Dredge Suction Systems

Figure | Page

INTRODUCTION

Of interest is the determination of the three-dimensional velocity field in the vicinity of a plain-ended suction pipe near a horizontal, solid boundary. The pipe is assumed to be located in an infinite reservoir to eliminate consideration of other boundary effects. The independent variables of primary interest are the pipe flowrate; the distance from the floor to the pipe opening; and the angle of the pipe from the vertical. In addition, the shape of the suction pipe inlet must be considered. A plain-ended opening was employed for these initial experiments. Since the entire velocity field was of concern, the type of inlet selected became of less concern for the far field effects. This paper describes the laboratory scale experimental results and compares them with the potential flow, theoretical solution for a three-dimensional point sink near a solid boundary.

COMPLETE PROBLEM SCOPE

The problem considered here is only the first step toward development of an understanding of a much more complex problem. Of primary concern is an understanding of the slurry intake and the flow field surrounding the cutterhead of a hydraulic dredging system. The front is piece depicts some typical dredge suction systems including the cutterhead type. In this case, the flowfield is also swirling due to the rotation of the cutterhead in the digging process; the suction opening may be elliptical and somewhat flared in the shape; the pipe opening is obstructed by the moving blades of the cutter; the surrounding

bottom geometry is not necessarily horizontal and continually changing during dredging; and the bottom is a movable-bed, soil material. Because of these complexities and the inherent scaling problems associated with laboratory tests of the soil-water interactions involved, it was decided to initially begin with the relatively simple problem scope described in this paper.

MOTIVATION AND APPLICATIONS

In a hydraulic dredging system approximately 15-20% of solids (by volume) is entrained in a turbulent suspension of water at the suction entrance pipe leading to the centrifugal dredge pump. The slurry is then usually pumped from the dredge via a pipeline to the disposal area. Very little is known about the basic mechanisms for material entrainment at the cutter intake. One possibility is that the cutter simply stirs up the soil and puts it into suspension so that it is swept into the suction opening before resettlement can take place. The turbidity cloud that surrounds a typical dredging operation indicates that some resuspended material escapes from the intake velocity field. Another possibility is that the rotating cutterhead blades lift and guide the material into the suction pipe opening. Possibly, some combination of these mechanisms exists depending upon the soil conditions, cutterhead design, rotation speed, suction opening location and other factors.

For many years dredgers showed little or no interest in this area. However, because dredging has recently been considered a source of pollution, (turbidity cloud reduces photosynthesis, creates local oxygen demand, etc.) they have become quite interested in ways to devise "clean" dredging systems. Reference 1 includes suggestions for studying new

cutterhead shapes and inlet opening locations to guide the material and improve the solids volume transported. Also, the possibility of shields or other devices are mentioned which contain and eliminate the turbidity cloud emanating from the digging area.

For these reasons therefore, this basic, introductory study was initiated. Of concern is the relative distance (radius) from the suction pipe to where the velocity field drops off to below the "escape" velocity for soil particles; the bottom velocity gradients which produce critical shear stresses to "move" the surrounding soil; and the location of flow separation zones which make the potential flow solution unrealistic.

LITERATURE REVIEW

There is little actual literature on the mechanics of the dredge suction inlet. Slotta (10) considered the flow field near and within a dredge cutterhead. However, the flow information obtained was qualitative and concerned improvements in cutter efficiency. Dredgers have made some broad evaluations by observing sediment movement (3) but precise analytical studies are lacking. Idealizing the fluid mechanics of this situation, the dredge suction inlet was considered as a finite sink near a solid boundary. Much fluid mechanics literature was reviewed with very limited results.

Some interesting literature in the field of rheology shed light on this study. Metzner, Uebler, and Chan Man Fong (7) compared the flow of a Newtonian fluid and a viscoelastic fluid from a large reservoir into a small tube. This paper concentrated on the inlet viscinity but did show photographs of the larger area indicating that all material in the Newtonian flow headed directly toward the inlet. Marrucci and Murch (6) developed the mathematics for flow from a reservoir to a circular orifice. Giesekus (4) studied the effect of a variety of inlet shapes on the flow fields of viscoelastic fluids. Uebler (11) considered the approaching flow field in his study of pipe entrance flow. Each of these sources consider Newtonian sink flow peripherally to their main subject. They indicate only that in Newtonian flow all movement is uniformly toward the inlet. None considered sink flow near a solid boundary. The experimental results presented were useful in a qualitative way only.

In order to develop theoretical flow field equations appropriate to this study, standard fluid dynamic methods were used (8,9,12). By using potential flow theory and the principle of superposition, a suitable theoretical math model was constructed. Verification of this model then proceeded using an experimental model and a suitable form of flow visualization. Modeling laws (5) and methods of flow visualization (1,2,10) were readily available.

EXPERIMENTAL APPARATUS

The parameters considered for the experimental apparatus of this experiment were size, lack of external disturbance, accessibility, and cost. The testing area had to be large enough to approximate an infinite reservoir. The fluid had to be removed and returned so that the depth was not a variable and external influences were small. Adequate accessibility was needed to view the experiment, take data, and adjust the equipment. Low cost was attained by using an inexpensive fluid and surplus parts and material when possible. The apparatus consisted of a tank containing one thousand gallons of water, a circulation pump, flow meters, and related plumbing.

The Tank

The tank (Fig. 1) is of heavy steel construction with a zink rich submarine primer and bright white finish coat to help reflect light. The test section is separated from the manifold sections by diffusers consisting of aluminum screen and linen. These diffusers worked quite well. At the maximum flow rate of 67 GPM (0.0119 CFS), the average return velocity was:

$$V = \frac{Q}{A} = \frac{0.0119}{16} = 0.00074 \text{ ft./sec.} \qquad (1)$$

The lowest velocity to be measured was on the order of 0.01 ft./sec. so the velocity of water returning to the test section was considered low enough not to disturb test results. A differential head of about a quarter inch was observed across the diffusers with a considerable

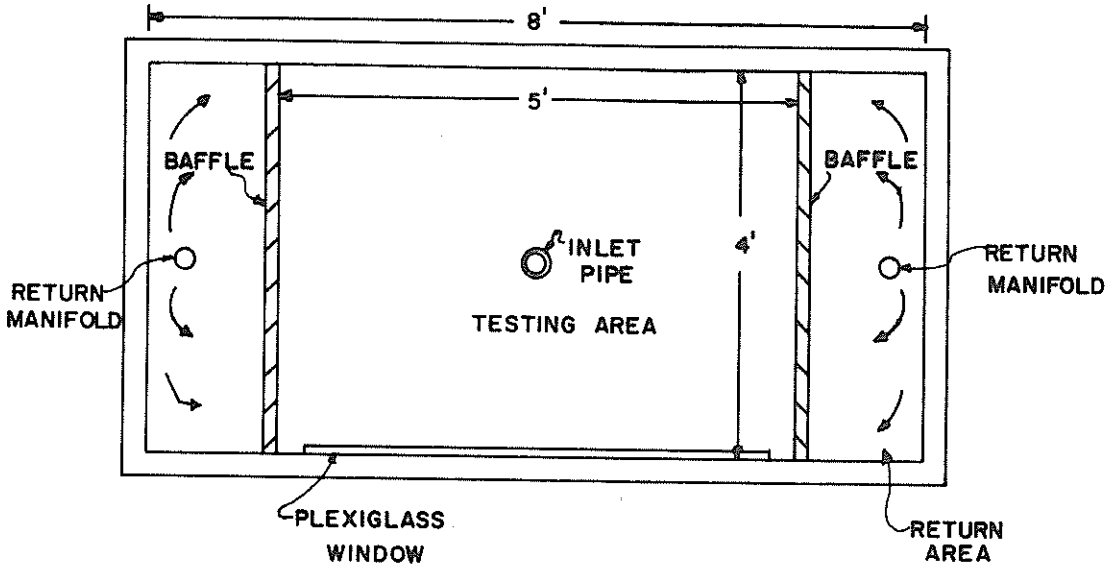

TOP VIEW

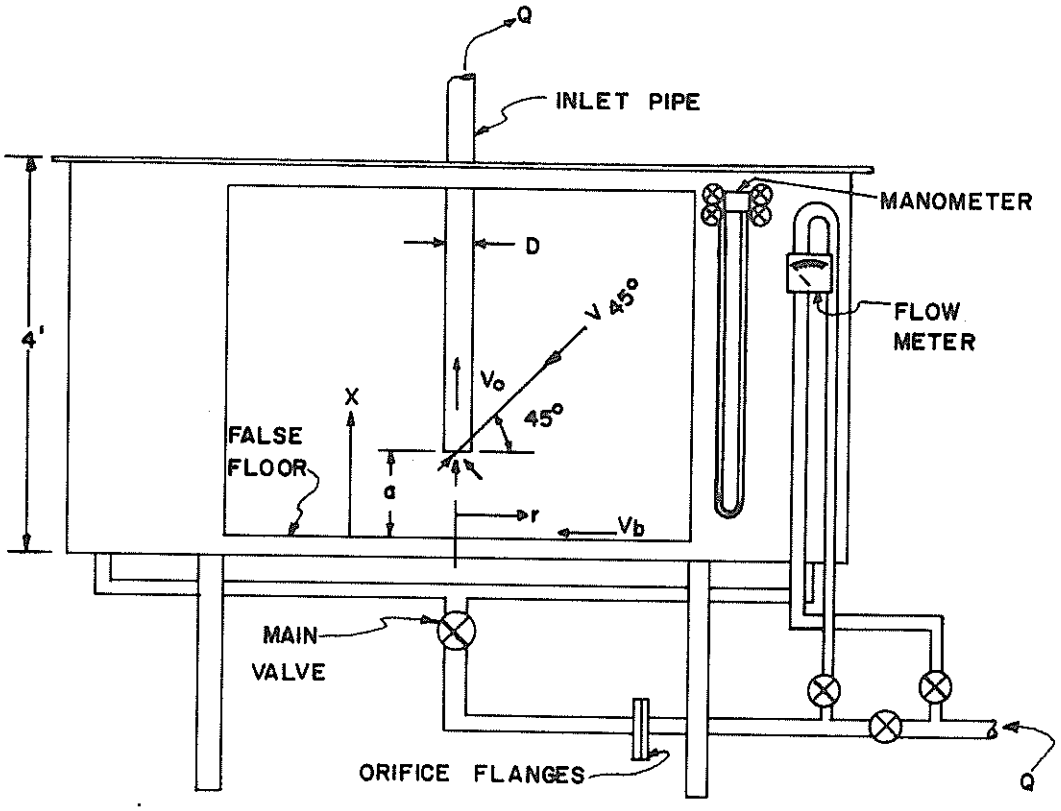

FRONT VIEW

Fig. 1 Experimental Apparatus

difference in turbulence level.

The test section was viewed through a 4 x 5 foot plexiglas window. A false bottom of plate glass was placed in the test section to provide a smooth, level working surface and to facilitate observations of water currents when the calmness of the tank was being checked. The back of the tank was covered with black cloth and a grid of contrasting white cord. Floodlights for photography were placed just above the surface of the water. The top of the tank was covered with canvas to keep dust out of the tank and to keep reflected light out of the working area in front of the tank.

Instrumentation

The fixed instrumentation located on the tank consisted of two flow meters, high and low range, and a high speed clock. The low range flow meter was a two inch, 75 gallon per minute commercially calibrated meter. This flow meter had a dial indicator readout and was mounted with valves so that it could be placed in line with the pump or bypassed. The high range flow meter was an orifice meter built for this investigation. The one inch orifice was placed in the two inch pipe between the pump and the manifold piping. A fifty inch mercury manometer gave the pressure difference taken by flange taps on both sides of the orifice. The theoretical orifice equation for this meter (at rates above 40 GPM) relating flow rate to pressure differential is:

$$Q = (157.7 \times h)^{\frac{1}{2}} \qquad (2)$$

where Q = flow rate, GPM

h = pressure, inches of mercury

After installation, the accuracy of this meter was checked against Eq. (2) and the commercially calibrated meter. Valving was set to place both flow meters in series. The main choke valve was adjusted to several flow rates and readings were taken from the dial indicator and manometer. Fig. 2 is a graphical representation of Eq. (2) and shows the data points provided by the two flow meters. The graph is full logarithmic and, assuming no compensating error exists, indicates that the orifice meter is quite accurate even for flow rates below 40 GPM.

The pump used for this experiment was only capable of moving 43.5 GPM through the low rate flow meter. With the reduced piping involved with the high range flow meter, a maximum flow rate of 67 GPM was attained. A pump with greater pressure and flow capacities would be desirable for future applications.

The high speed clock used was positioned beside the camera and was viewed by the camera through a plate glass mirror. The clock was marked in .001 second intervals. The 8mm film produced a slightly blurred image but could easily be read to .01 second accuracy.

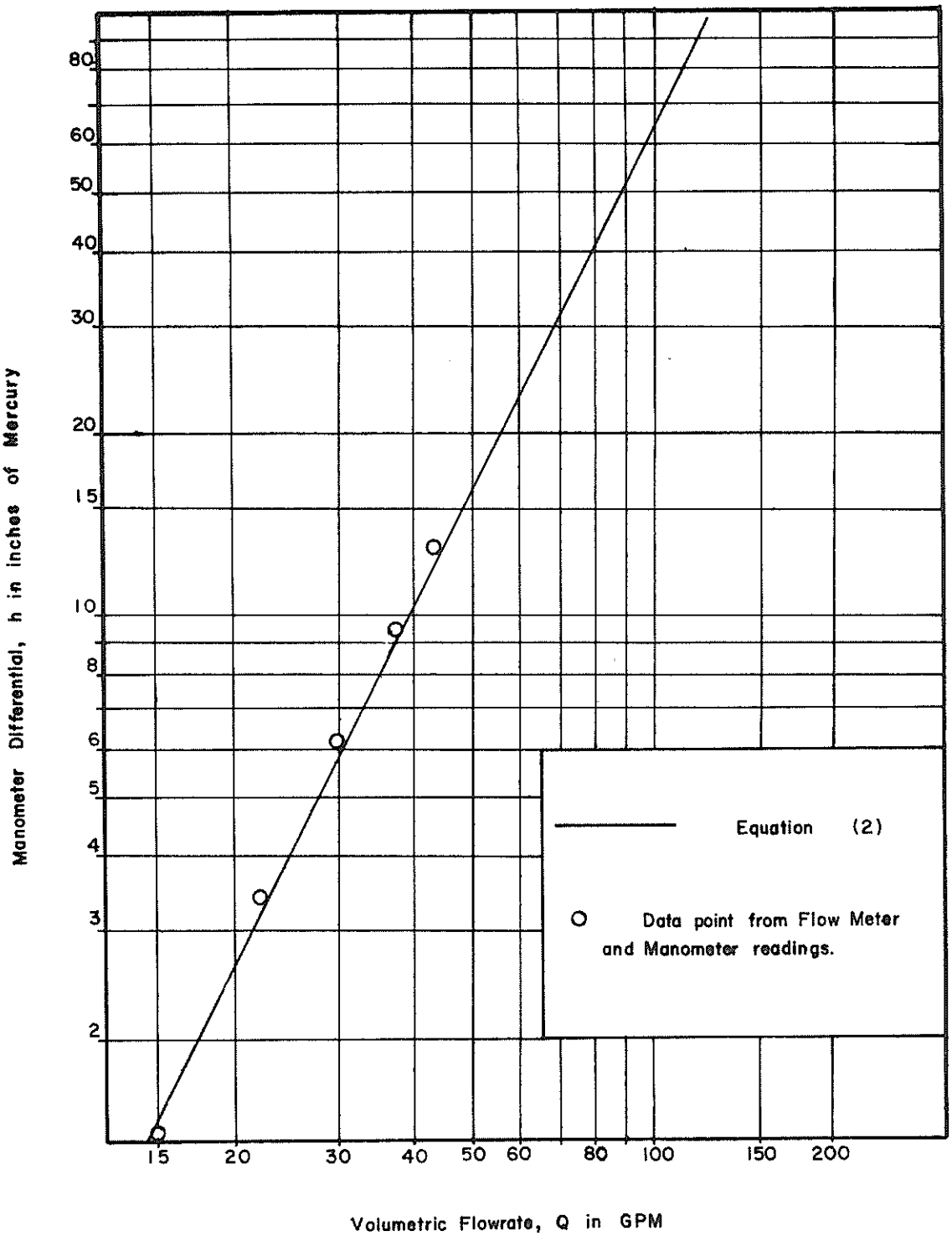

Fig. 2 Orifice Meter Flow Rate Curve

DATA COLLECTION

The objective of this experiment was to detect with reasonable accuracy and minimum disturbance the flow field around a three dimensional, single suction inlet. The problem was to determine the velocity and direction of each particle of fluid at any time. That is, to visualize the flow both quantitatively and qualitatively. The upper limit on velocity was conceived to be about 20 feet per second at the inlet. The lower limit of velocity that could be measured with any degree of accuracy was predicted to be about .01 feet per second. This represents three orders of magnitude, an ambitious range of measurement.

Several methods of flow visualization were investigated before an adequate system was developed. A hot film anemometer was first considered. This sophisticated equipment was readily available in Texas A&M University's Hydromechanics Laboratory. However, for this study a hot film anemometer was too sensitive, too delicate, and sampled too small an area. Next, the hydrogen bubble technique was investigated. This method in conjunction with photography can sample a large area (2). The main shortcoming concerns the buoyancy induced convection currents created by a large number of these bubbles which can obscure results where velocities are small. The very small velocities involved in this study disqualified this method.

Buoyant Oil

Indicator oils are made for instruments with specific gravities of 1.2, 1.0, and 0.875. These oils are compatible and with a little practice a person can mix them to match the specific gravity of water at various temperatures to within 0.0001 S.G. The oil can be made nearly perfectly neutrally buoyant.

The oil was injected into the water near the area of interest by an oil rake (Fig. 3), a manifold of 3/16 inch brass tubes. The oil was bright red and formed beads of about 1/4 inch to less than one sixteenth inch diameter. The oil was delivered to the rake through a 1/4 inch nylon plastic tube connected to a common pump type oiler can. The squeeze lever on the pump was fitted with an adjustable stop to limit its travel. The pump was squeezed with the minimum force and travel to just release oil beads of the desired size and quantity.

This method was developed in a beaker sized apparatus. When it was transferred to the thousand gallon tank, it did not work. Several times the oil was carefully balanced, pumped through the plastic tube to the oil rake and the experiment begun, only to have the oil become lighter as the experiment progressed. After several ruined tests, it was discovered that the clear plastic Tygon brand tube was slightly soluble in the oil and given enough time and the six foot length of tube, significant changes in density occurred. A change in specific gravity of 0.001 was completely unacceptable as it caused a quarter inch drop of oil to move due to buoyancy at about 0.02 feet per

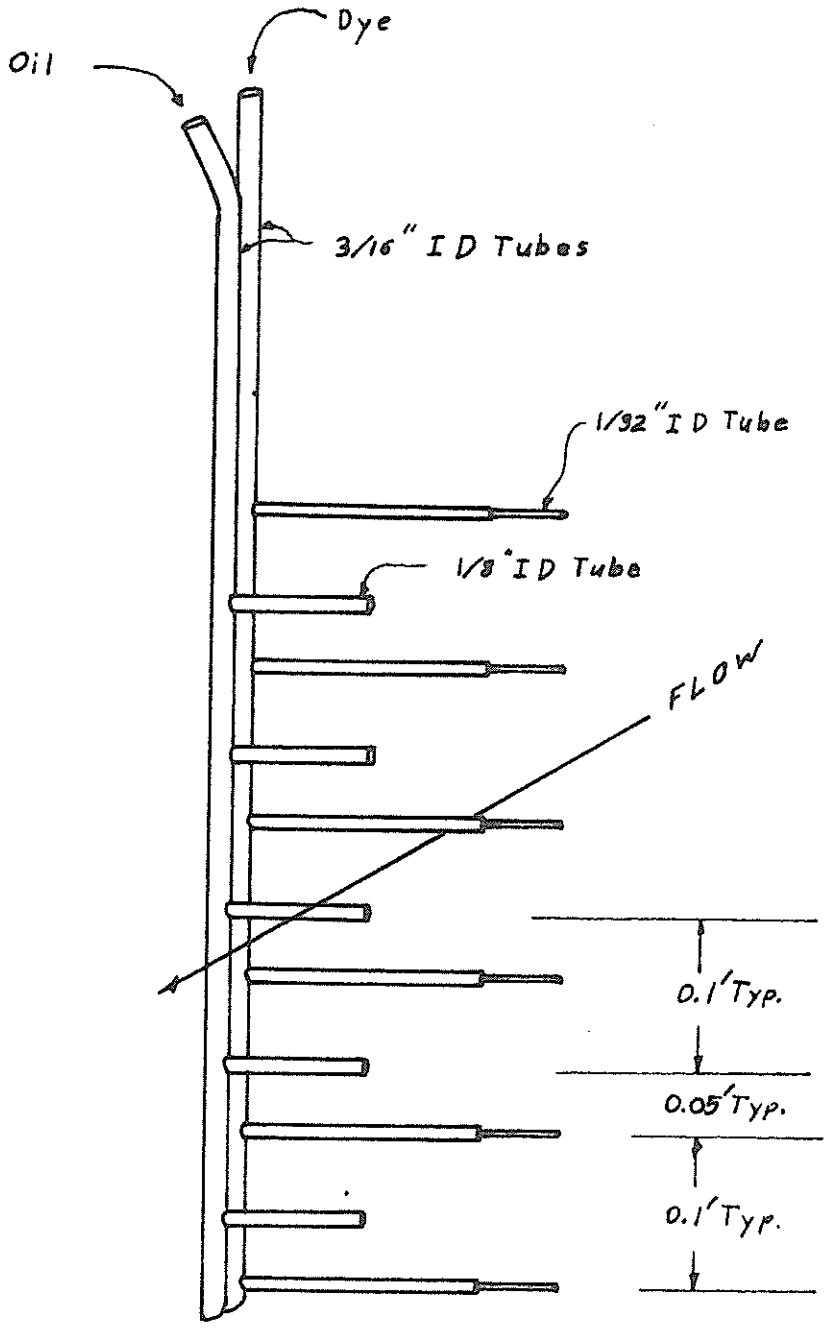

Fig. 3 Indicator Rake

second. At this point, the nylon plastic tube was substituted with satisfactory results. As a result of these difficulties, a quick back flush procedure was developed where the oil in the tube was bled by hydrostatic pressure into a second container and the tube flushed by water. The oil was removed from the water and reused. Fresh oil was pumped back through the tube and testing continued.

The buoyant oil showed excellent possibilities for recording the speed and direction of fluid flow. The red beads were easily recorded on color film and the velocity range that could be recorded was limited only by the lighting and speed of the camera used. The visual observation of the oil beads also gave a good feel for the processes occurring in the flow.

A negative feature of this buoyant oil technique in a recirculating system was the clouding of the water by the emulsified oil. Linen bags tied around the return manifolds were unable to filter most of the oil that had been finely divided by the turbulence of the pump and plumbing. Even with the energy input from the pump and floodlights, the water temperature never varied enough during testing to require rebalancing of the oil before it became necessary to change the water due to poor visibility. Because of the time required to change the water and rebalance the oil, the oil was used frugally.

Dye Streaks

Dye dispensed from a given point for a period of time represents a streak line. For steady state conditions, this is also a stream

line. Bright green, 1.00 specific gravity, water base indicating fluid was used. It was mixed double strength with water in a one liter beaker from which it was fed by gravity through flexible tubing to the dye rake. A pinch valve regulated the flow and a hemostat quickly switched the flow on or off. A combination oil and dye rake (Fig. 3) was constructed to dispense the two indicating fluids simultaneously.

The dye streaks were to serve as a check on the unreliable oil beads. However, the combination resulted in a system that expedited the acquisition of the desired data considerably. The highly reflective dye could be used sparsely and clouded the water only slightly. The fact that the stream lines in many cases were well defined resulted in a much lower usage of the oil and resulting problems. The dye rake and dye were used as a check on the calmness of the tank. If a small quantity of dye was released and remained in small balls at the tips of the dye rake, then the water was very still and testing could begin. If the puffs moved then the relative motion of fluid in the tank could be evaluated. During testing with the dye rake in very low velocity areas, the use of oil beads could be avoided completely. The flexible tube delivering the dye could be lightly pinched below the regulation valve causing a puff and then a gap in the streak line. As a test run was being conducted and the test area became more and more disturbed, a point of instability was reached in which the dye produced no distinguishable streak line but was mixed by general turbulence. This and preceding stages could be monitored by observing

the dye streaks. The dye lines in general gave a good visual "feel" for the flow field and it was the dye which greatly facilitated the interpretation of the transient phenomena of this experiment.

Data Recording

In order to determine directly the velocity of flow at a given point, it is necessary to measure the displacement of a particle at the point for a given period of time. The particle had been established as an oil bead or dye puff. A desirable method for recording velocity data photographically would be to use a single frame of film and multiple exposures. The timing of the exposures provides the time line and displacements can be measured from a single print. However, it was found that due to scattered light only a few exposures would be made before previous records were completely obscured. Therefore, a single exposure multiple frame system was used.

In order to take a nearly unlimited amount of data, an 8mm movie camera was chosen. Color film was used to better record the red oil. Powerful photo floodlights were placed above the water to provide light for photography and visual observation. An accurate clock was placed within the photographic frame to provide a time line. This method required an intricate data reduction technique but worked quite well.

The camera used can be operated to take single frames by presenting the desired apperature and triggering the shutter with a cable release placed in a special receptacle on the camera. In this way, more or fewer exposures could be taken depending on the situation.

However, it was found to be more practical to run the camera on full automatic. In this way, there was less chance of ruining the record by not having the proper exposure or enough frames of data. Excess frames were skipped over during data reduction. Also, the camera had a fairly accurate framing rate which facilitated data reduction. The zoom lens and camera position relative to the tank were set and not disturbed throughout testing, again to reduce the difficulties of data reduction..

The clock used to establish the time line, a scientific type timer readable to 0.001 second, was placed beside the camera and was viewed through a mirror. Placed within the camera's field of focus and provided with its own illumination, the face of the timer was recorded in the corner of each frame of film exposed. The sweep hand moved so fast that it was just a blur on the film but could still be read to 0.01 second. Identification cards were placed beside the timer and were recorded in the adjacent corner of each photographic frame.

Data Reduction

The first step of data reduction was to inspect and transfer information from the thousands of frames of movie film to paper. The grid on the back of the tank was used to get relative locations and to check for distortion, which turned out to be slight. The diameter of the inlet tube was carefully measured and was used to determine the relative scale of the photographic record. A special data sheet was

prepared containing a true scale on the bottom and a grid similar to the one seen on the film. Because of its small size, a microfilm viewer was used to inspect the eight millimeter film. For data reduction, the viewer was modified by removing its translucent screen and using it as a projector. The pertinent frame was then projected onto a data sheet using the grid for reference and the required time and position information was transferred directly. Of the thousands of frames run, several hundred were selected and transferred to about two hundred data sheets which were then consolidated to nine sheets for the nine flow conditions tested.

Experimental Procedure

The experimental procedure that was used, both preliminary and actual, is listed with a brief description of each step. The purpose of this section is to illustrate the actual procedures and techniques involved.

Setting the inlet. The position of the inlet tube was established as desired. The height of the inlet was physically measured and the setting of the point gauge recorded.

Balancing oil. After the tank had been filled, the room and water temperature were measured and recorded. A water sample was taken in a large beaker. The specific gravity of the sample was measured with a hydrometer to within 0.0005. The density of the water varied from day to day with variations in dissolved solids and gases, suspended solids, and temperature.

The range of specific gravities encountered were 0.9955 to 0.9980 for water temperatures between 90°F and 72°F. The hydrometer was placed in a graduated cylinder and the specific gravity adjusted up or down to within 0.001 by mixing lighter or heavier oils with the 1.00 S.G. oil. Additional adjustment was then made by dripping drops of oil into the beaker of water and noting their relative movement. If the larger drops remained close to very small drops or pieces of lint, the oil was neutrally buoyant. A final test was made by repeating this step in the tank itself. This procedure had to be repeated each time the tank was refilled.

Mixing dye. The indicator dye was mixed double strength with water in a beaker suspended above the test tank.

Recording equipment. The camera was loaded and set. The position and operation of the mirror and clock were checked. Cards identifying a particular test run were placed beside the clock.

Indicator rake. The oil was pumped through the nylon tube to the oil rake. The dye was fed from its beaker by siphon and gravity flow through the tube to the dye rake. The flow rate of the dye was adjusted with a pinch clamp and then the flow was shut off by pinching the tube with a hemostat.

Test Run

A typical test run consisted of taking flow data over a small area covered by one position of the indicator rake, one flow rate, and one inlet height and orientation. The steps followed one another

in rapid succession. A test run required just a few minutes with a fifteen to thirty minute wait between runs for the water in the tank to become calm again.

Previous run. The indicator rake, flow rate, and appropriate cards were set up in the preliminary procedures or previous test run.

Calmness. The relative calmness of the tank was checked by releasing a small amount of dye and observing its movement. If the motion was small, testing proceeded. If not, a wait of another five minutes was required.

Start. The clock was turned on, the pump started, and the dye hemostat released.

Data taking. When the dye streaks had just about established themselves, the floodlights were turned on. The camera was run for a few frames to identify the run and record the streak lines only. Oil beads or dye puffs were then released and the camera run a few seconds at intervals during the run.

Shut off. When enough data had been taken, the apparatus was shut down by shutting off the lights, clock, and dye.

Reset. The flow rate, identification cards, indicator rake and inlet pipe were reset as required. The test cycle was complete when the tank became calm enough to begin another test run.

THEORETICAL RESULTS

In order to analytically study the flow field of a dredge suction inlet near a solid boundary, a suitable model must be constructed. The flow inside the inlet pipe has been well established (4,7,11). The flow at any distance from the inlet may possibly be predicted by potential flow theory. This theory neglects viscous effects and is limited to axisymmetric cases in three dimensions.

Complex cases may be constructed from basic types of flow by the theory of superposition. A suction pipe of finite dimensions in an infinite reservoir could be modeled by integrating vertical doublets throughout the volume of a vertical right circular cylinder of semi-infinite length. This would produce an unwieldly expression. At distances large compared to its diameter, this inlet pipe would resemble a simple point sink. Since the primary interest of this study was the flow field several diameters from the inlet, a point sink was used to obtain the analytical results.

For a simple point source or sink, the equations are (12):

$$\psi = \frac{-mx}{(x^2 + r^2)^{\frac{1}{2}}} \quad , \quad \phi = \frac{-m}{(x^2 + r^2)^{\frac{1}{2}}} \qquad (3)$$

These equations give stream surfaces (surfaces of constant ϕ) and velocity potential surfaces (surfaces of constant ψ) as a function of position in the flow field in cylindrical coordinates. The x direction is along the vertical axis of symmetry. The r direction is horizontal out from the axis of symmetry. Because of axisymmetry,

the third coordinate, θ, need not be specified. The sign convention used here produces results consistent with conventional cartesian coordinate practices. The value m is the strength of the source or sink and is positive for a source and negative for a sink. For three dimensional flow, m is related to the flow rate, Q, by: $m = Q/4\pi$, (12). As can be readily seen, these equations represent conical surfaces for constant ψ-values and concentric spheres for constant ϕ-values.

For a simple point source or sink a distance, a, above the origin, the equations are (8):

$$\psi = \left[\frac{-m\,(x-a)}{[(x-a)^2 + r^2]^{\frac{1}{2}}}\right] \tag{4}$$

$$\phi = \left[\frac{-m}{[(x-a)^2 + r^2]^{\frac{1}{2}}}\right] \tag{5}$$

By superposition, that is, adding the expressions for a point source or sink at x = a and x = -a, a plane of symmetry is formed. This plane contains the origin and is perpendicular to the axis of symmetry. Because the flow field below the plane of symmetry is a mirror image of that above, no flow takes place across this plane and it represents a solid boundary. The equations become:

$$\psi = -m\left[\frac{x-a}{[(x-a)^2 + r^2]^{\frac{1}{2}}} + \frac{x+a}{[(x+a)^2 + r^2]^{\frac{1}{2}}}\right] \tag{6}$$

$$\phi = -m\left[\frac{1}{[(x-a)^2 + r^2]^{\frac{1}{2}}} + \frac{1}{[(x+a)^2 + r^2]^{\frac{1}{2}}}\right] \tag{7}$$

By considering only the flow above the plane of symmetry, these equations represent the flow field of a source or sink a distance, a, above a solid frictionless boundary. The components of velocity, V_x in the x direction and V_r in the r direction, are obtained by differentiating as follows (12):

$$V_x = \frac{1}{r}\frac{\partial \psi}{\partial r} = \frac{\partial \phi}{\partial x} \tag{8}$$

$$V_r = -\frac{1}{r}\frac{\partial \psi}{\partial x} = \frac{\partial \phi}{\partial r} \tag{9}$$

Carrying out the differentiations, these expressions become

$$V_x = m\left[\frac{x-a}{[(x-a)^2 + r^2]^{3/2}} + \frac{x+a}{[(x+a)^2 + r^2]^{3/2}}\right] \tag{10}$$

$$V_r = m\left[\frac{r}{[(x-a)^2 + r^2]^{3/2}} + \frac{r}{[(x+a)^2 + r^2]^{3/2}}\right] \tag{11}$$

The values of ϕ, ψ, V_x, V_r, or V may be determined at any point by substituting the values of x and r into the appropriate equation. In order to plot constant value lines for ϕ, ψ, or V, it is necessary to solve the equations for one of the independent variables as a function of the dependent variable and other independent variables. The resulting equations are cumbersome and have no explicit solutions. Numerical methods must be used to solve them.

Computer programs were written to solve these equations for the coordinates of constant ϕ-lines, constant ψ-lines, and constant V-lines and are given in Appendix III. Six plots for two flow rates and three sink positions are shown in Figs. 4 through 9. These

a = 0.117 ft.
m = -0.0089 CFS

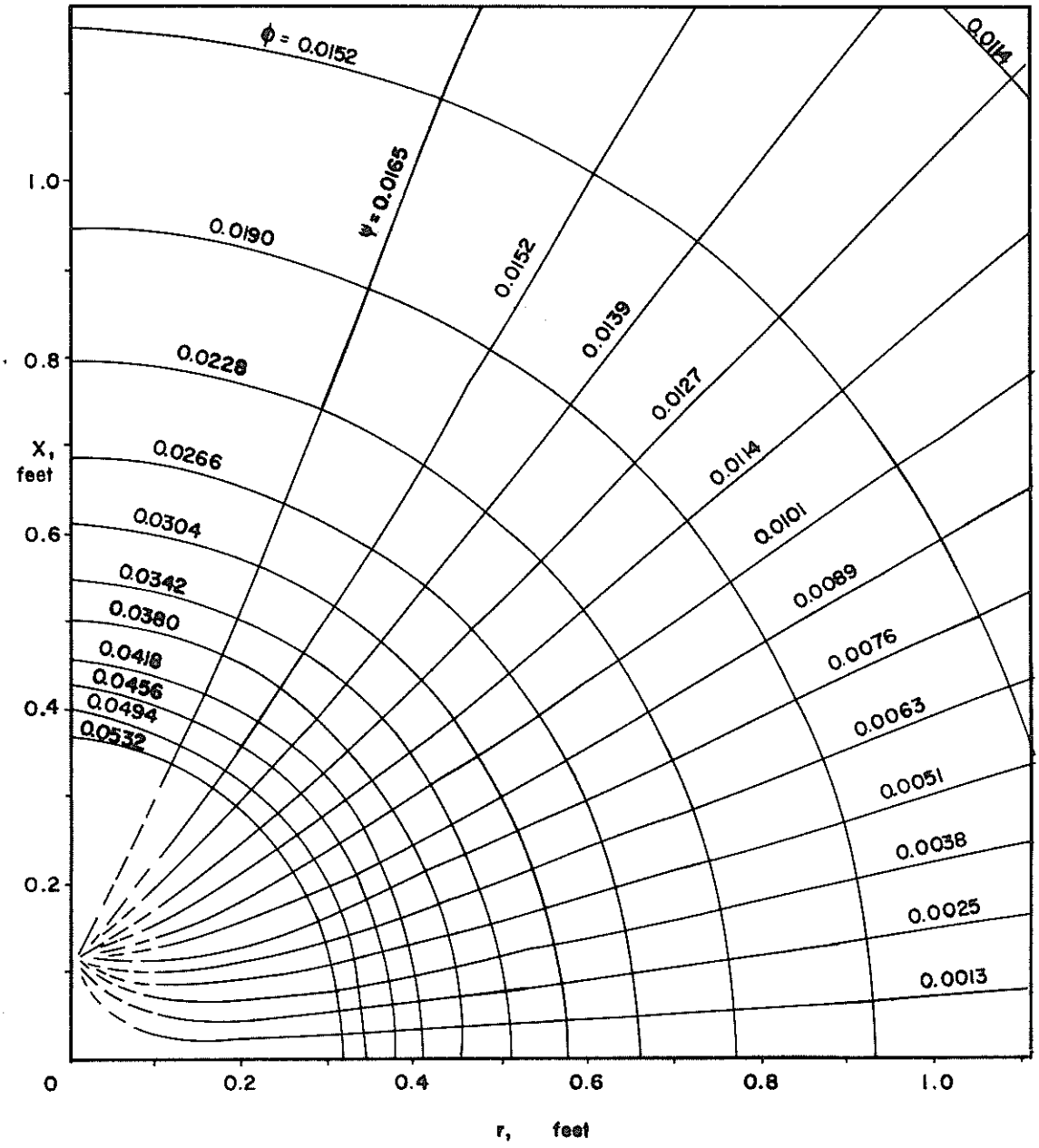

Fig. 4 Theoretical Sink Flow, a/D = 1.0, Q = 50 GPM

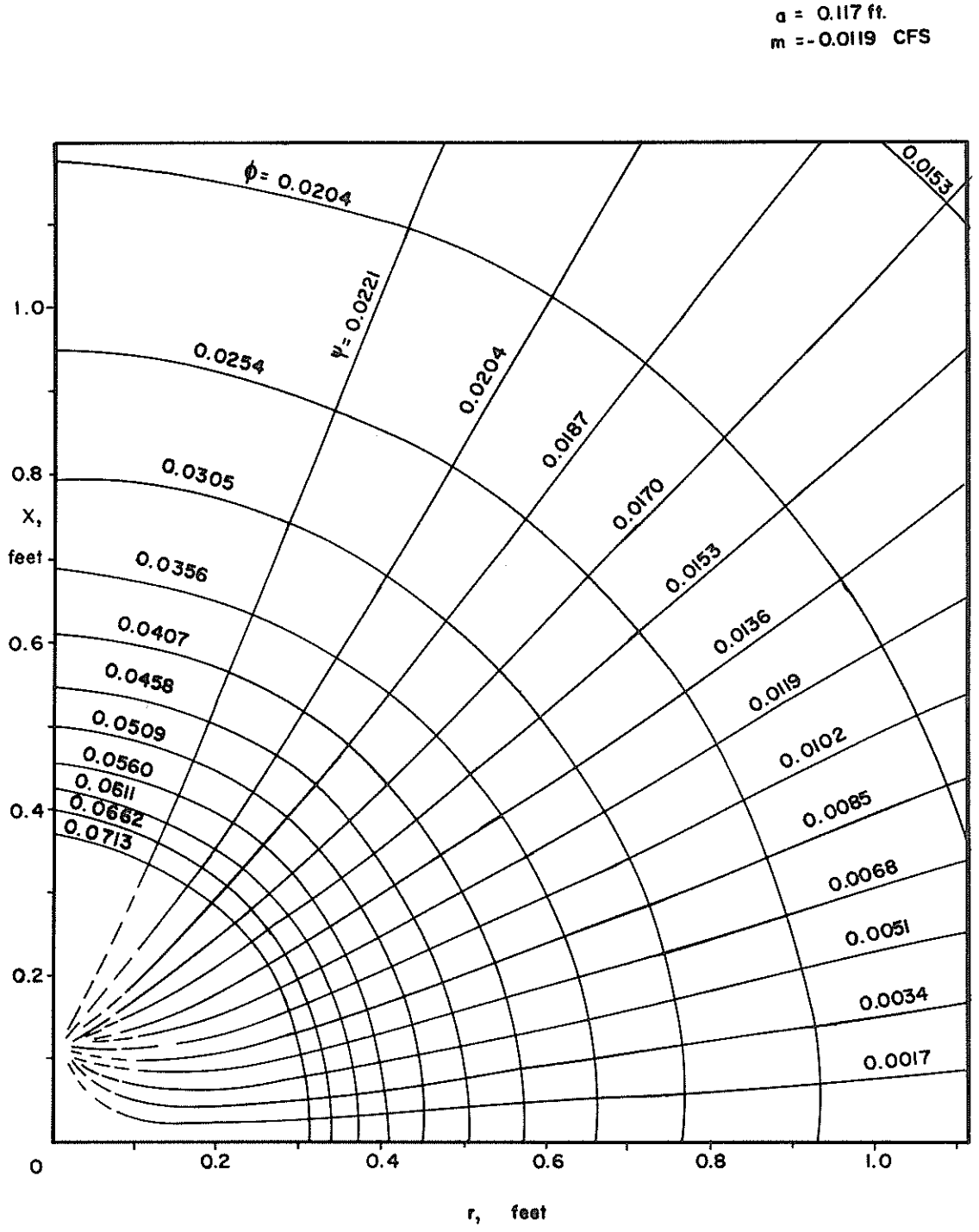

Fig. 5 Theoretical Sink Flow, a/D = 1.0, Q = 67 GPM

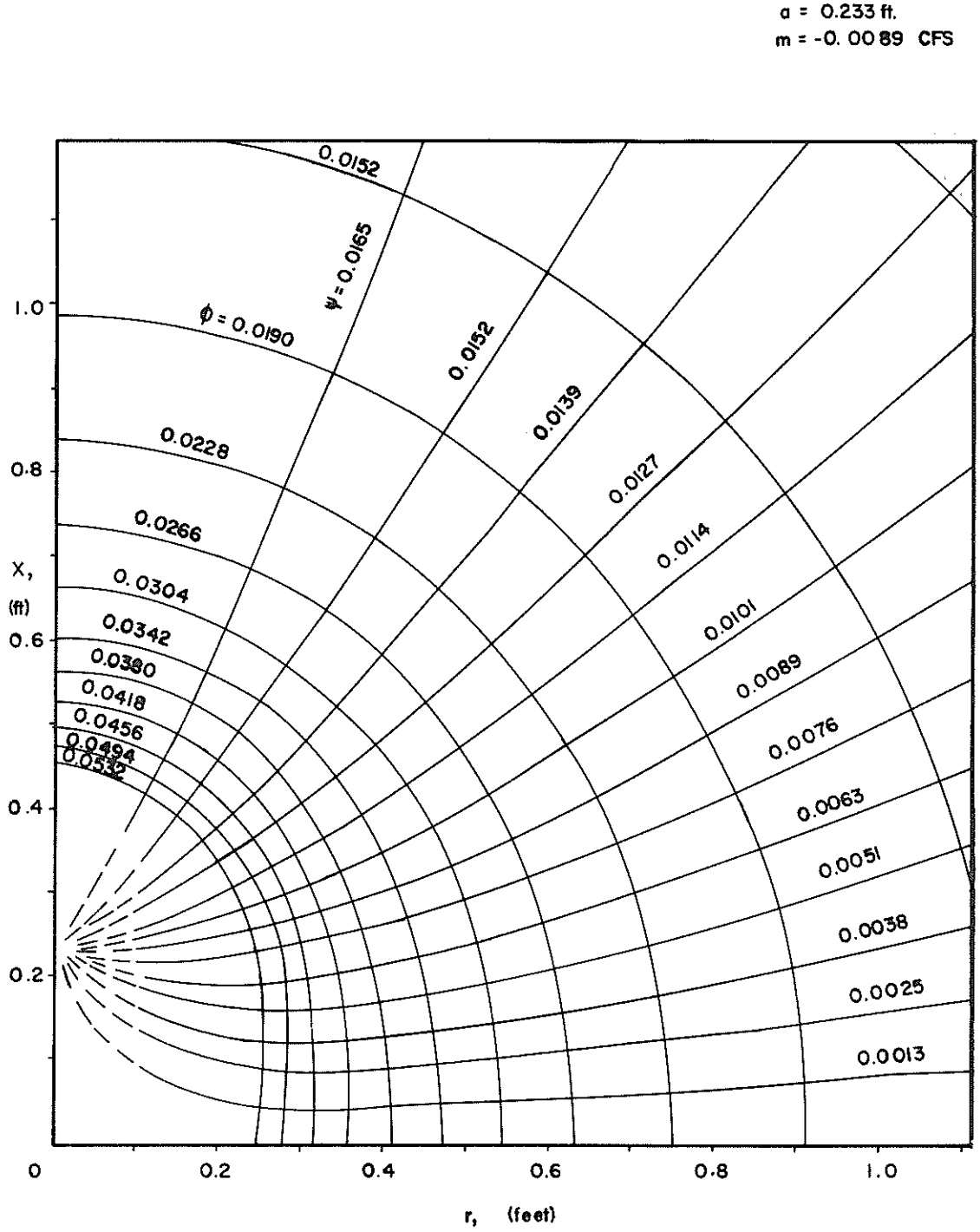

Fig. 6 Theoretical Sink Flow, a/D = 2.0, Q = 50 GPM

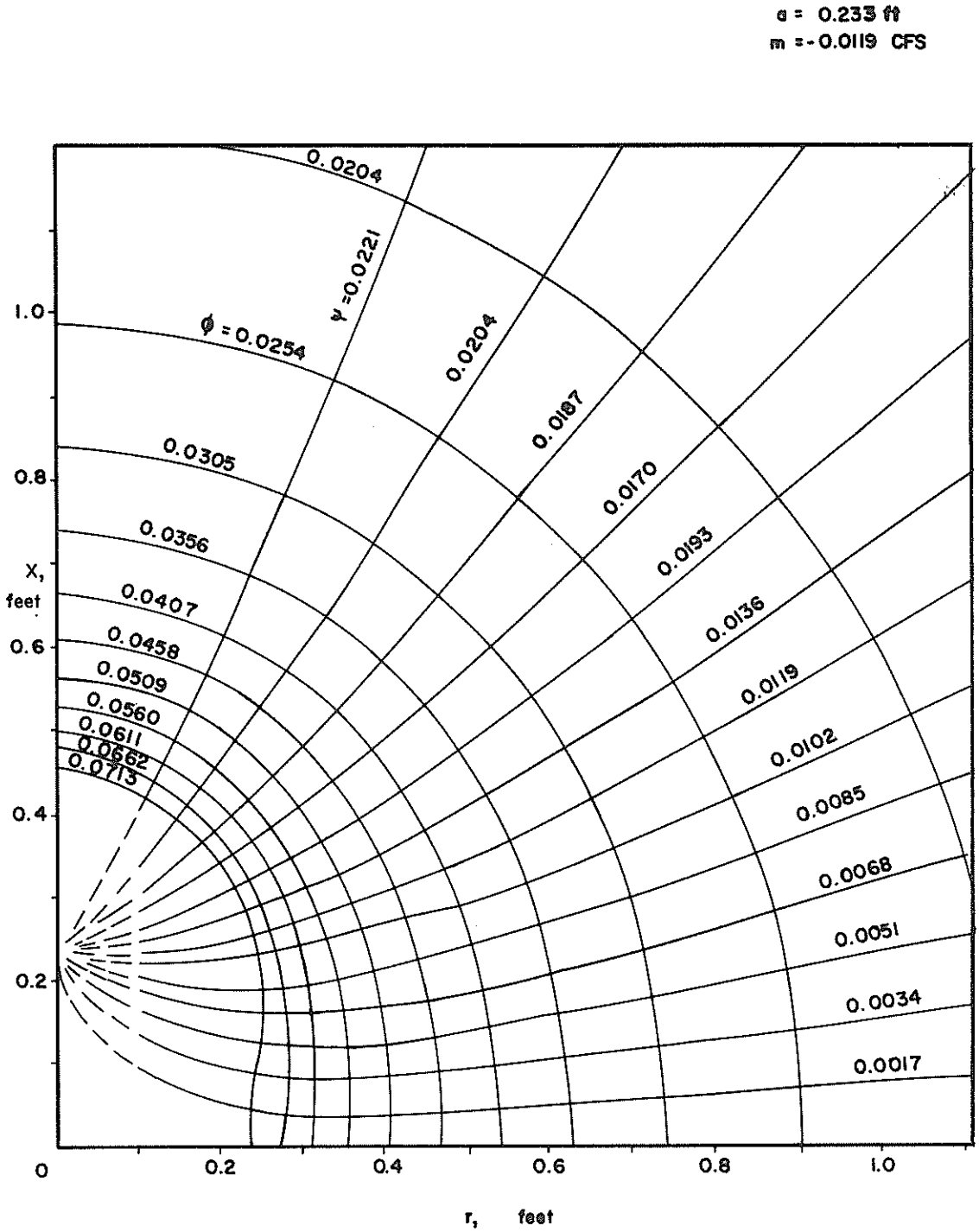

Fig. 7 Theoretical Sink Flow, a/D = 2.0, Q = 67 GPM

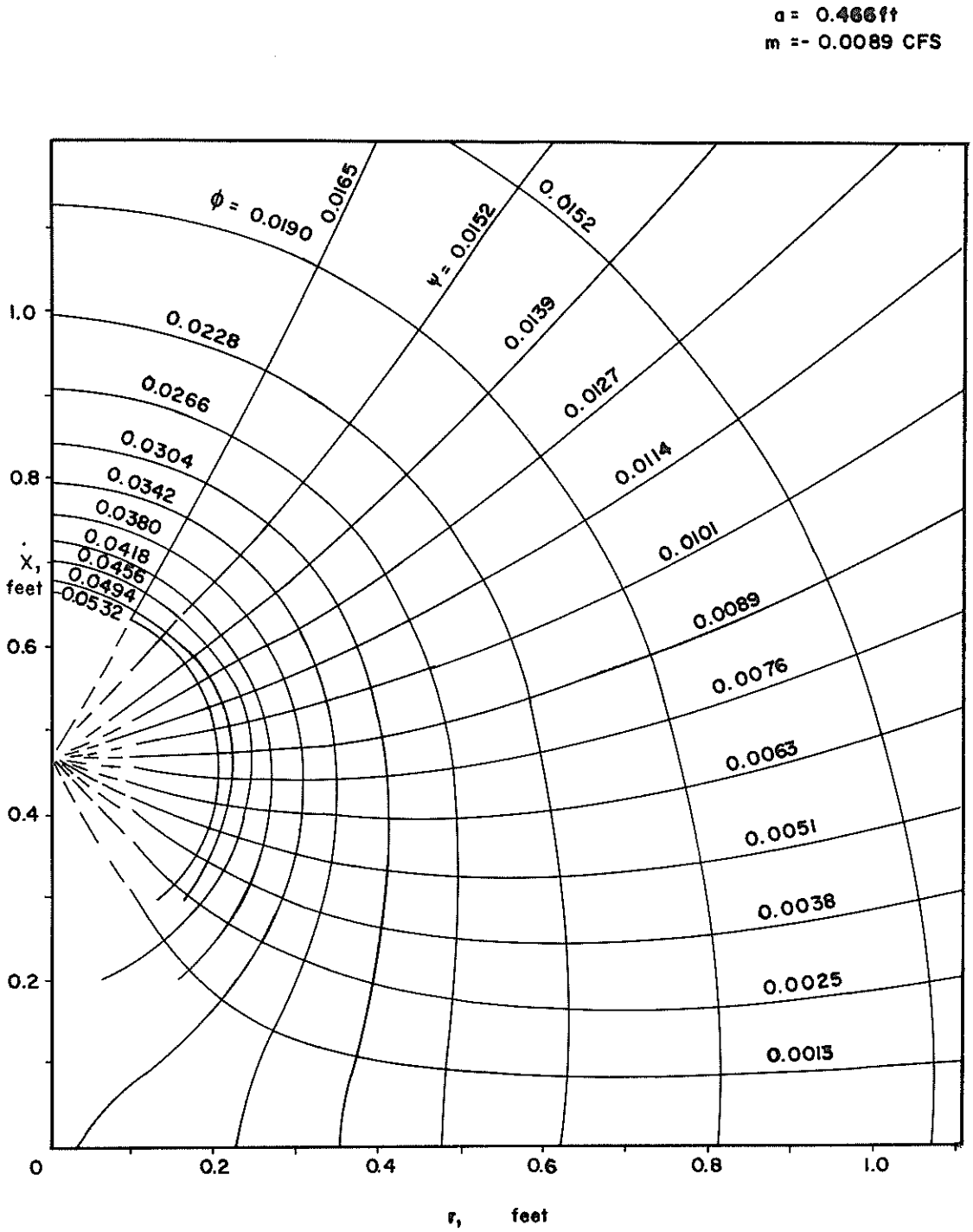

Fig. 8 Theoretical Sink Flow, a/D = 4.0, Q = 50 GPM

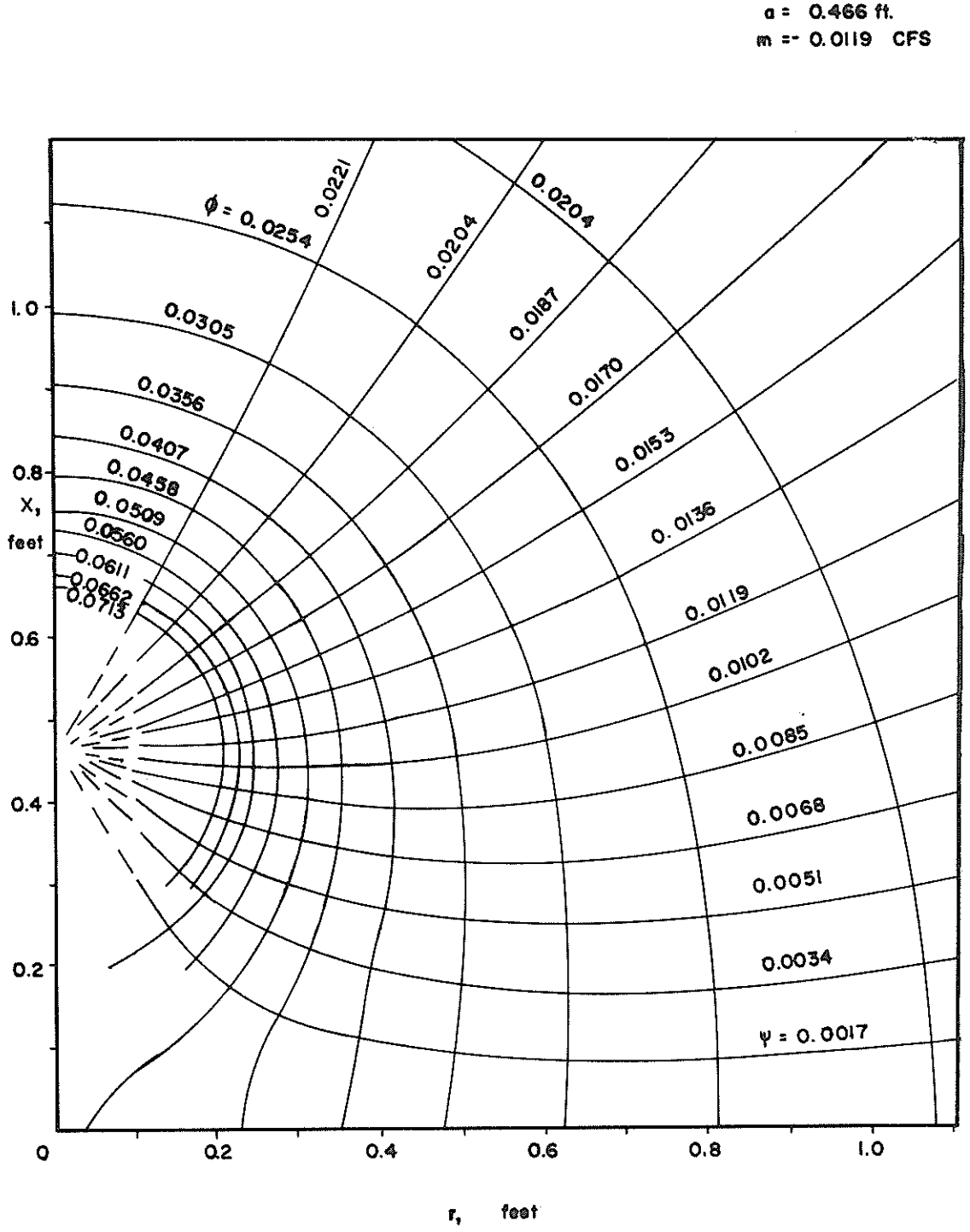

Fig. 9 Theoretical Sink Flow, a/D = 4.0, Q = 67 GPM

figures show a first quadrant section of a three dimensional field. Values for the constants a and m were chosen to correspond to experimental values. Constant velocity lines will be shown later in conjunction with experimental results.

Some points about these flow fields are worth noting. Different flow rates produce similar flow fields with only the values of ψ and ϕ differing for a given sink location. The part of the x-axis above the sink is one stream line. The positive r-axis plus the part of the x-axis between the origin and the sink is another stream line. Note how the space between the x-axis and the next stream line is much larger than the spacing between subsequent stream lines. The explanation is that these ϕ and ψ-lines represent surfaces of rotation about the x-axis. The velocity of flow is inversely related to the volume of space encompassed by adjacent ϕ and ψ surfaces. Equal volumes correspond to equal velocities. This is similar to the two-dimensional situation where the area between adjacent ϕ and ψ-lines is inversely related to velocity.

In general, this potential flow model of a dredge suction inlet suggests that all flow is toward the sink with displacement of flow caused by the flat surface. For a real fluid such as water it would be expected that viscous effects would further modify the flow, especially near the solid boundary.

EXPERIMENTAL RESULTS

In order to physically model a dredge, suction inlet modeling laws must be followed. The variables of this experiment are inlet velocity V_o, inlet diameter D, inlet height from the bottom a, water density ρ, water viscosity μ, and a distance L. L is an unspecified dimension term which can represent any distance such as x or r. A dimensional analysis of these values using the Buckingham Π Theorem (5) was performed, producing a Reynolds number, N_r, and two dimensionless length terms:

$$\Pi 1 = \frac{\rho D V_o}{\mu} \tag{13}$$

$$\Pi 2 = \frac{a}{D} \tag{14}$$

$$\Pi 3 = \frac{L}{D} \tag{15}$$

Therefore, Reynolds similarity should be used when scaling the results of this experiment.

Nine separate cases were considered in this experiment. Two flow rates and three inlet heights were used on a vertical suction pipe. The flow field in front, beside and behind a suction pipe at 45° to the vertical and at a single flow rate was also recorded. Diameter of the inlet pipe was 0.117 feet. Heights of the inlet pipe above the bottom were multiples of this diameter. Flow rates used were chosen arbitrarily with the maximum rate of 67 GPM (0.15 CFS) producing an inlet velocity of 16 ft./sec. ($N_r = 2 \times 10^5$).

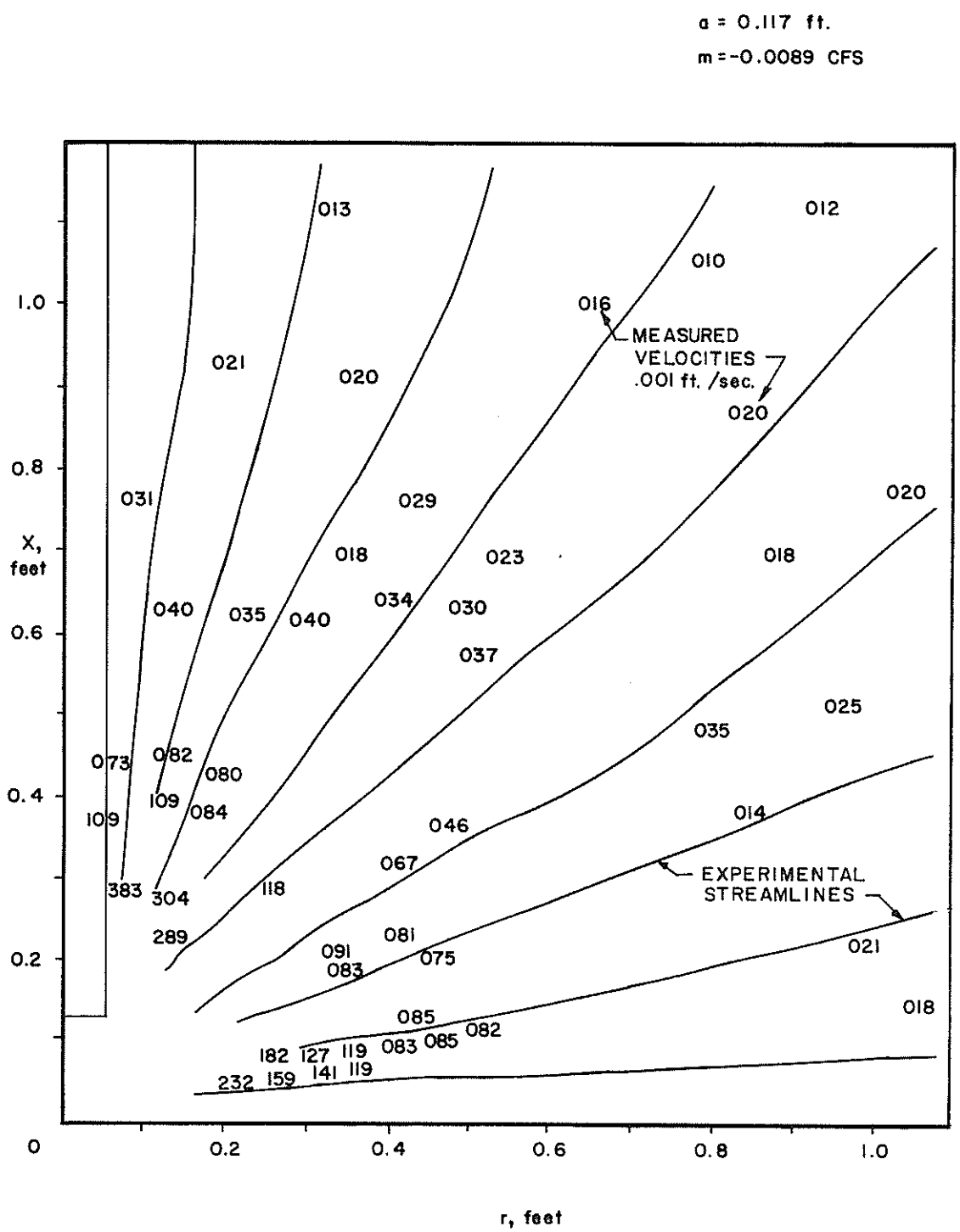

Fig. 10 Experimental Sink Flow, a/D = 1.0, Q = 50 GPM

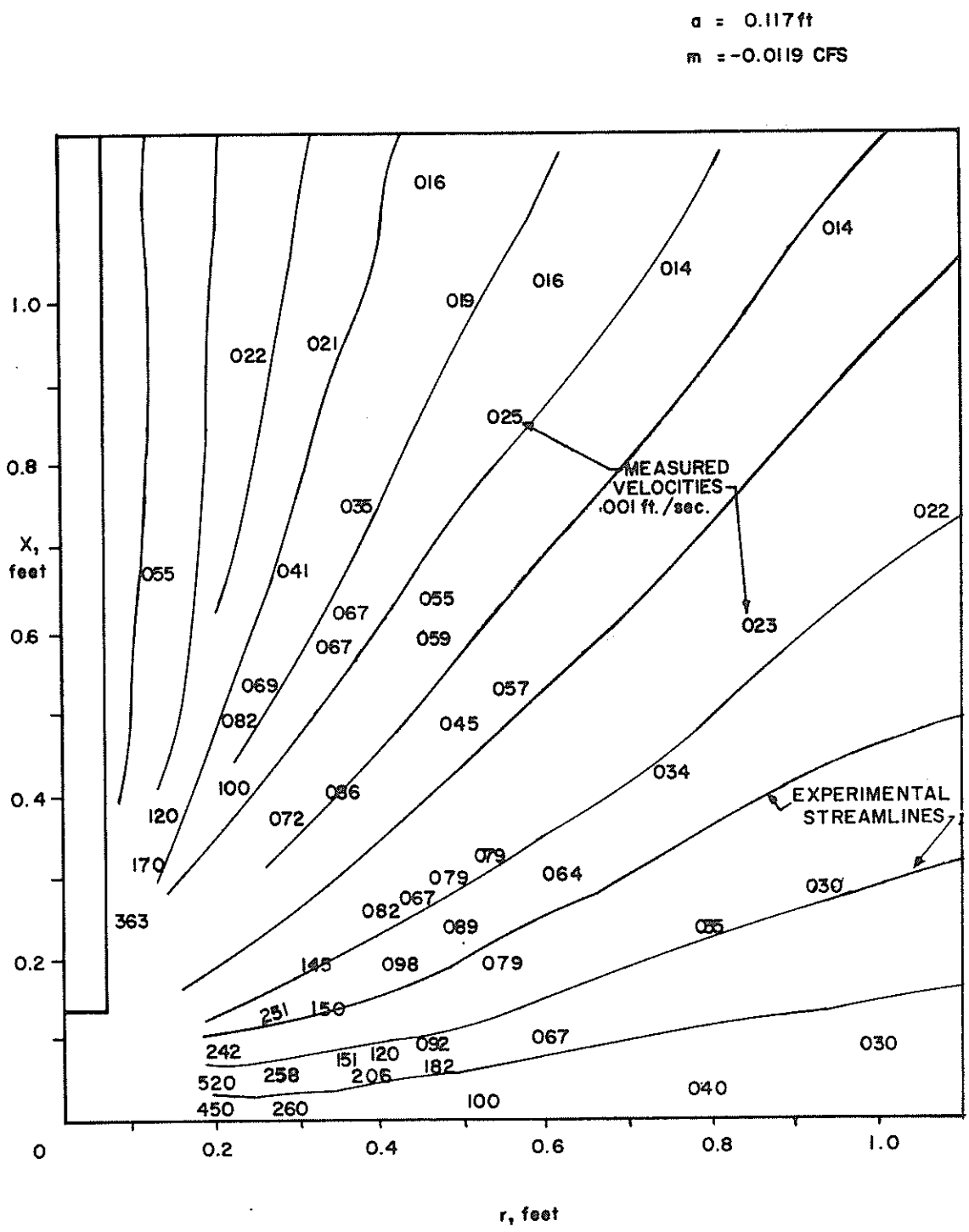

Fig. 11 Experimental Sink Flow, a/D = 1.0, Q = 67 GPM

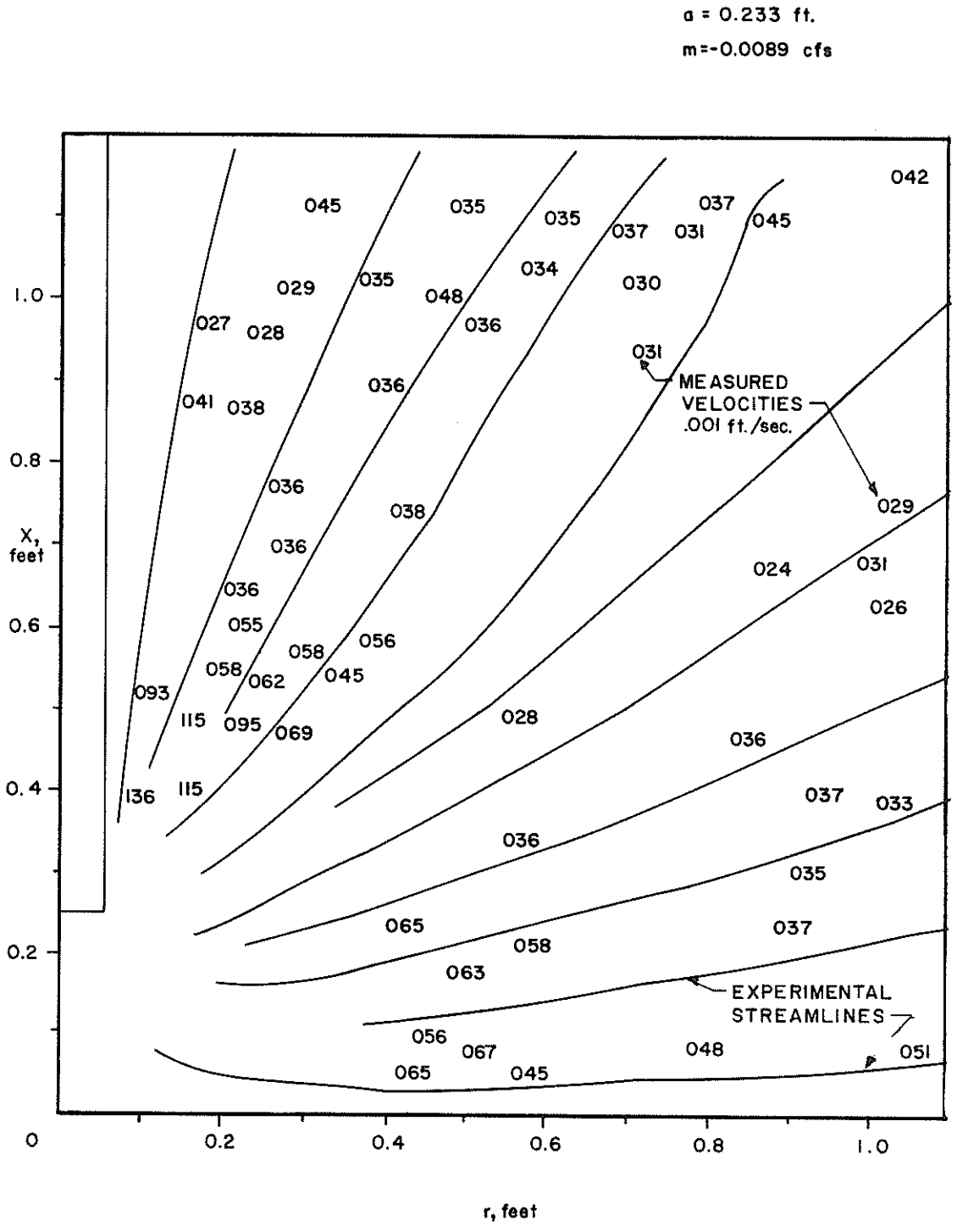

Fig. 12 Experimental Sink Flow, a/D = 2.0, Q = 50 GPM

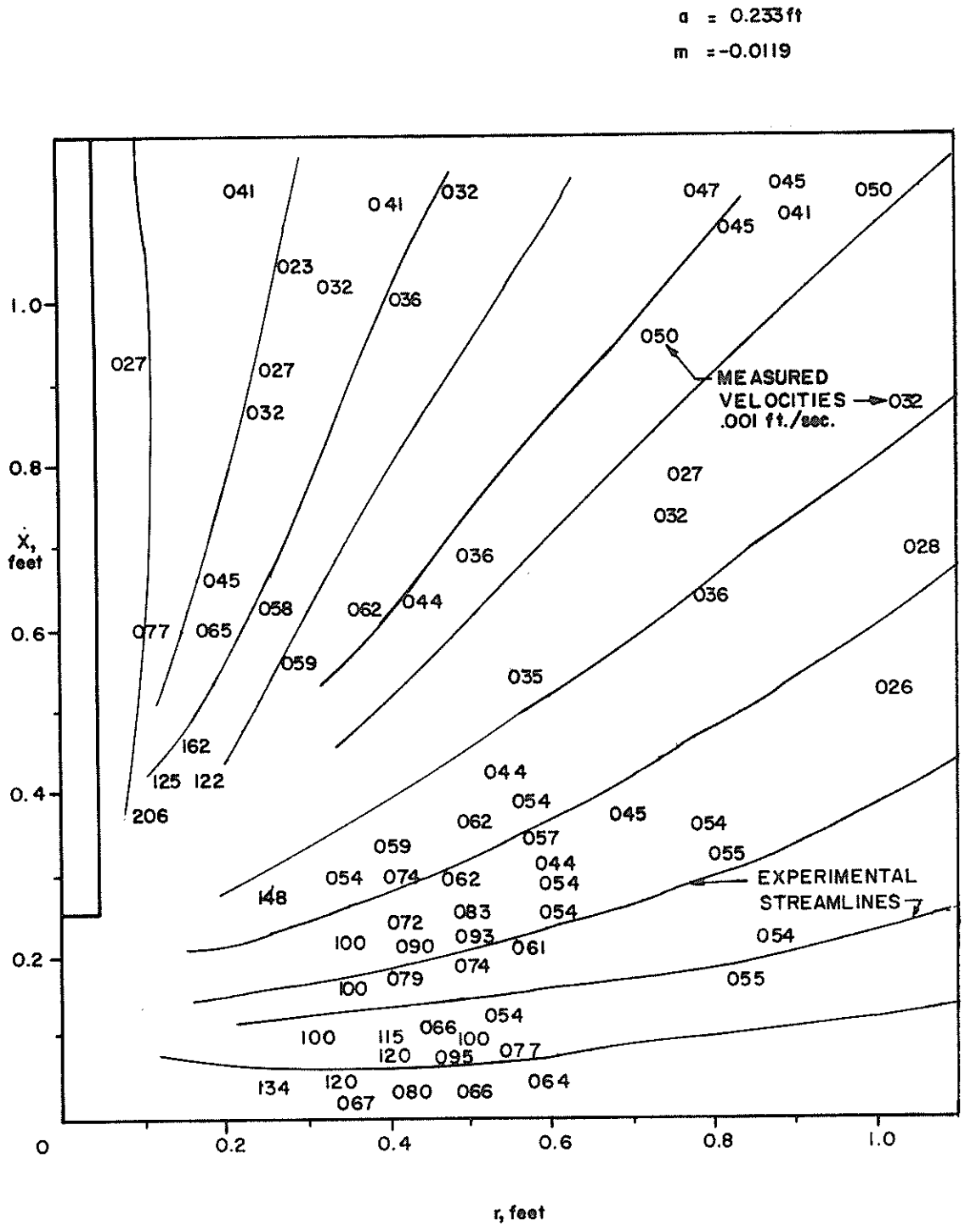

Fig. 13 Experimental Sink Flow, a/D = 2.0, Q = 67 GPM

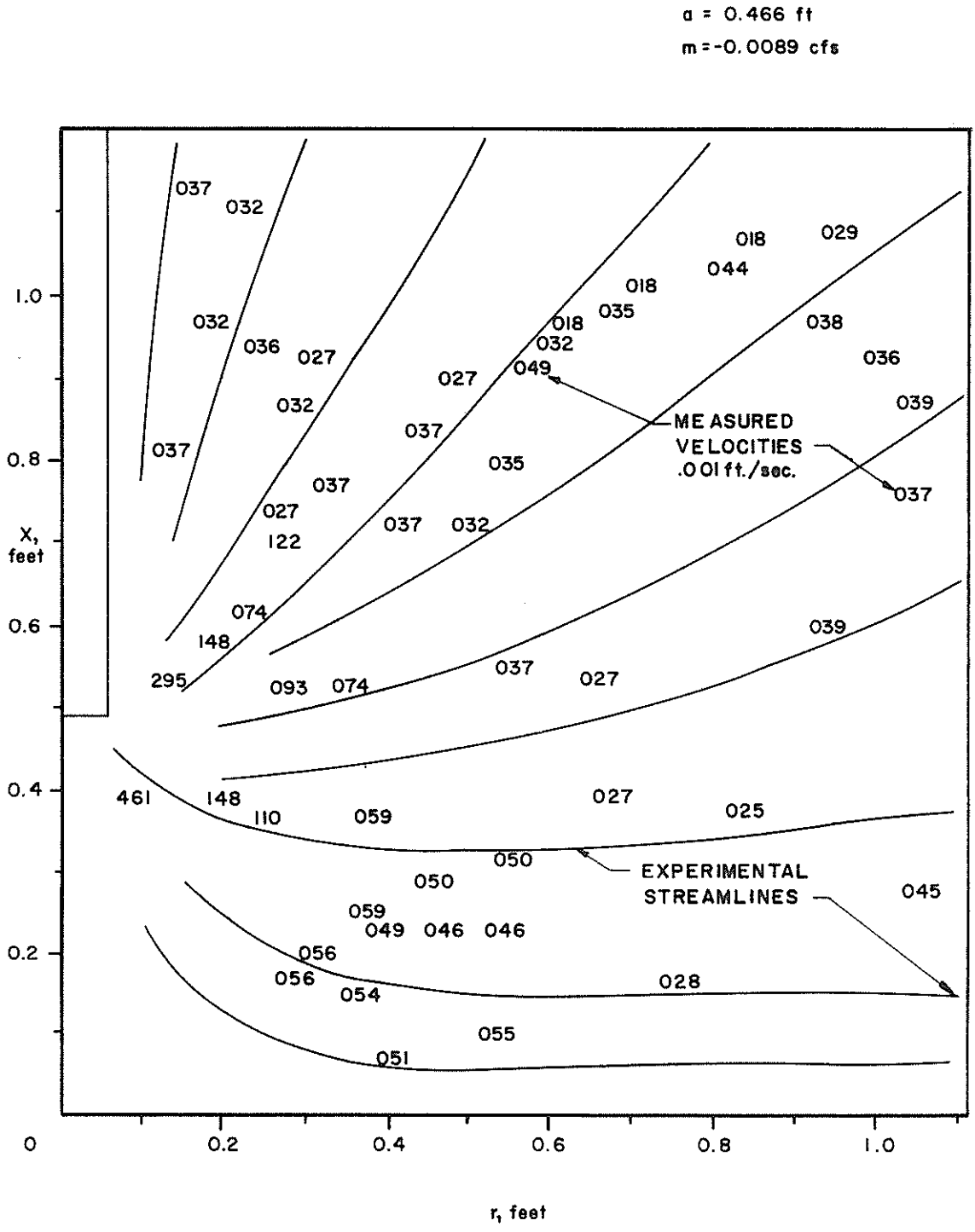

Fig. 14 Experimental Sink Flow, a/D = 4.0, Q = 50 GPM

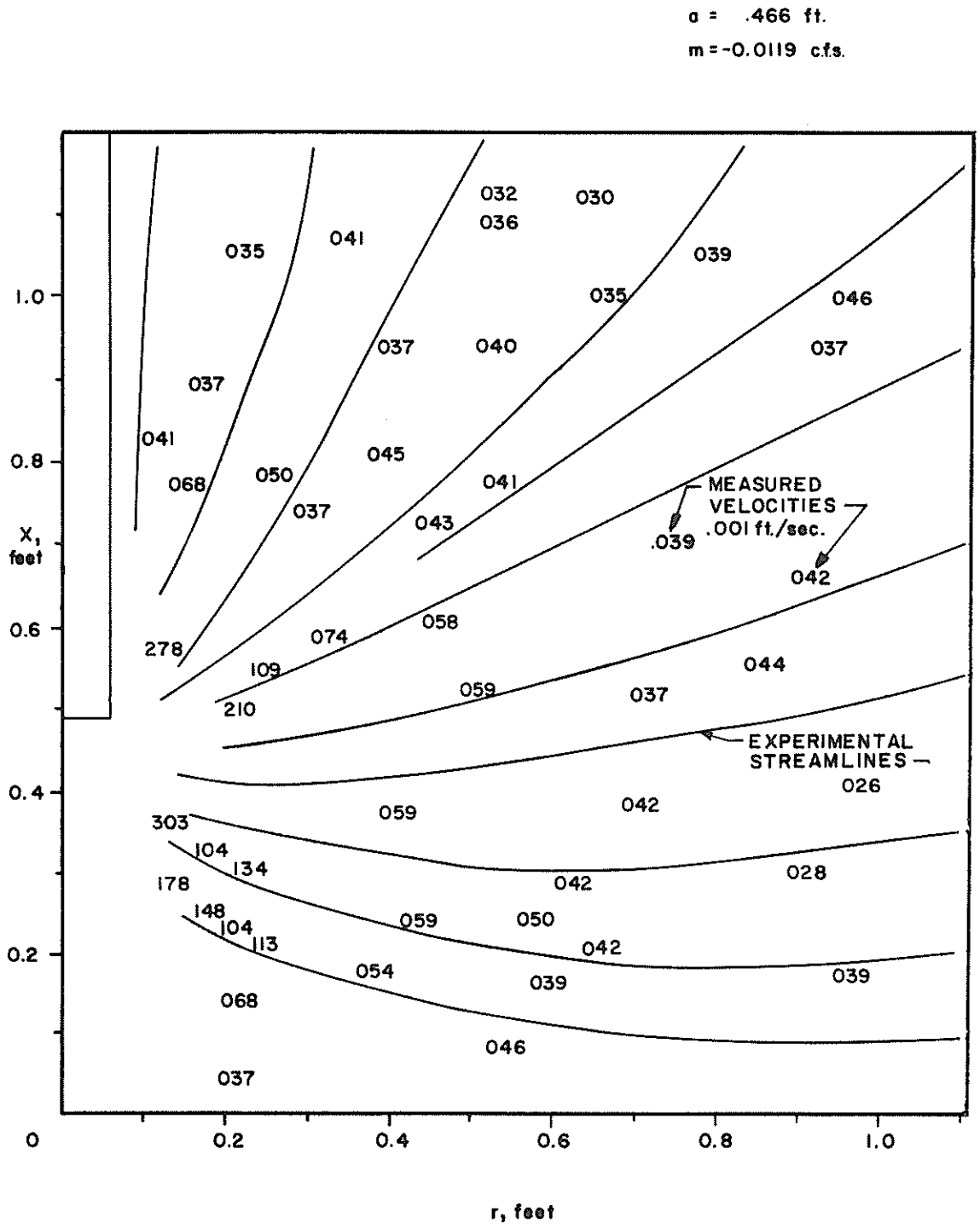

Fig. 15 Experimental Sink Flow, a/D = 4.0, Q = 67 GPM

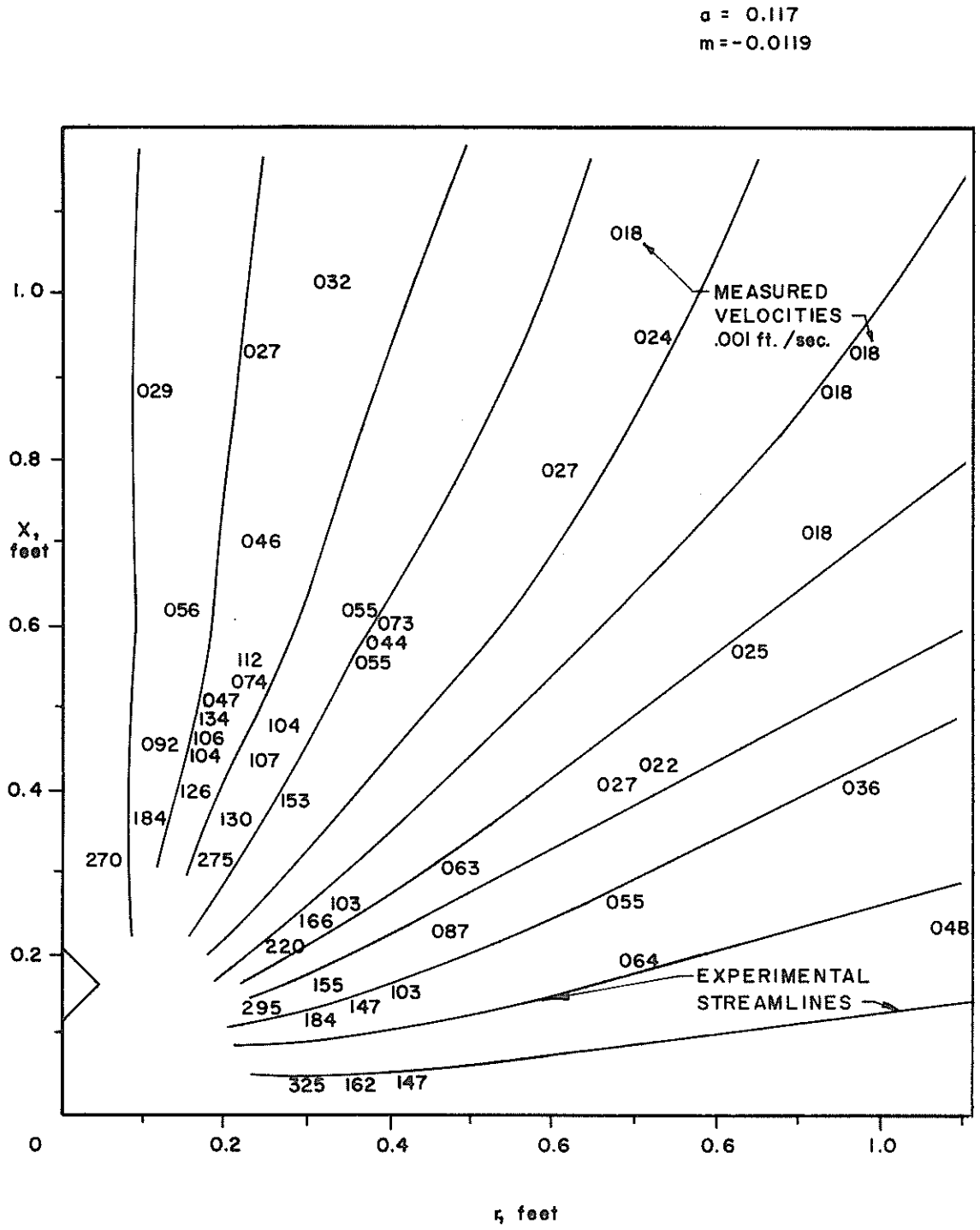

Fig. 16 Experimental Sink Flow, Front, $\theta = 45°$, $a/D = 1.0$, $Q = 67$ GPM

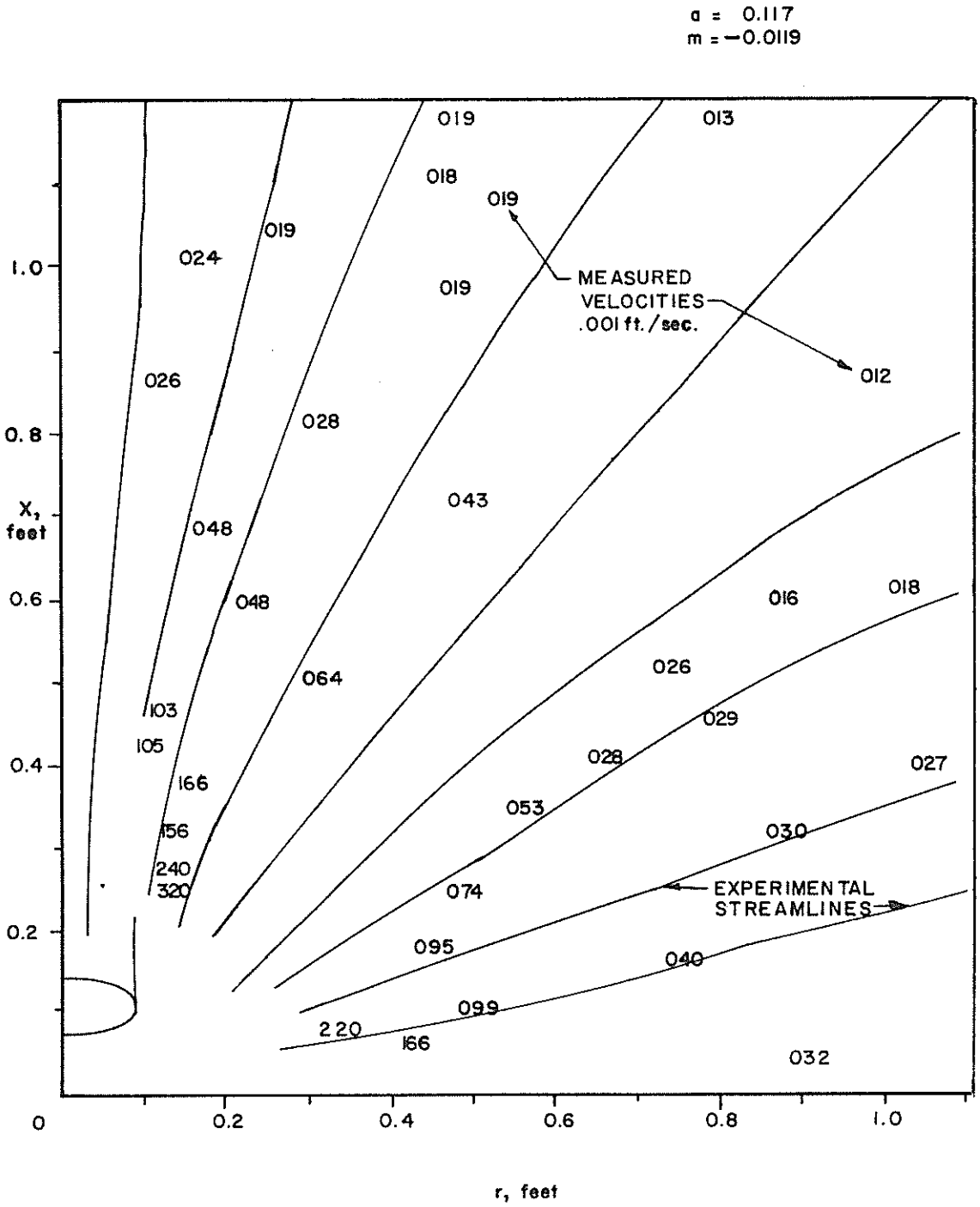

Fig. 17 Experimental Sink Flow, Side, θ = 45°, a/D = 1.0, Q = 67 GPM

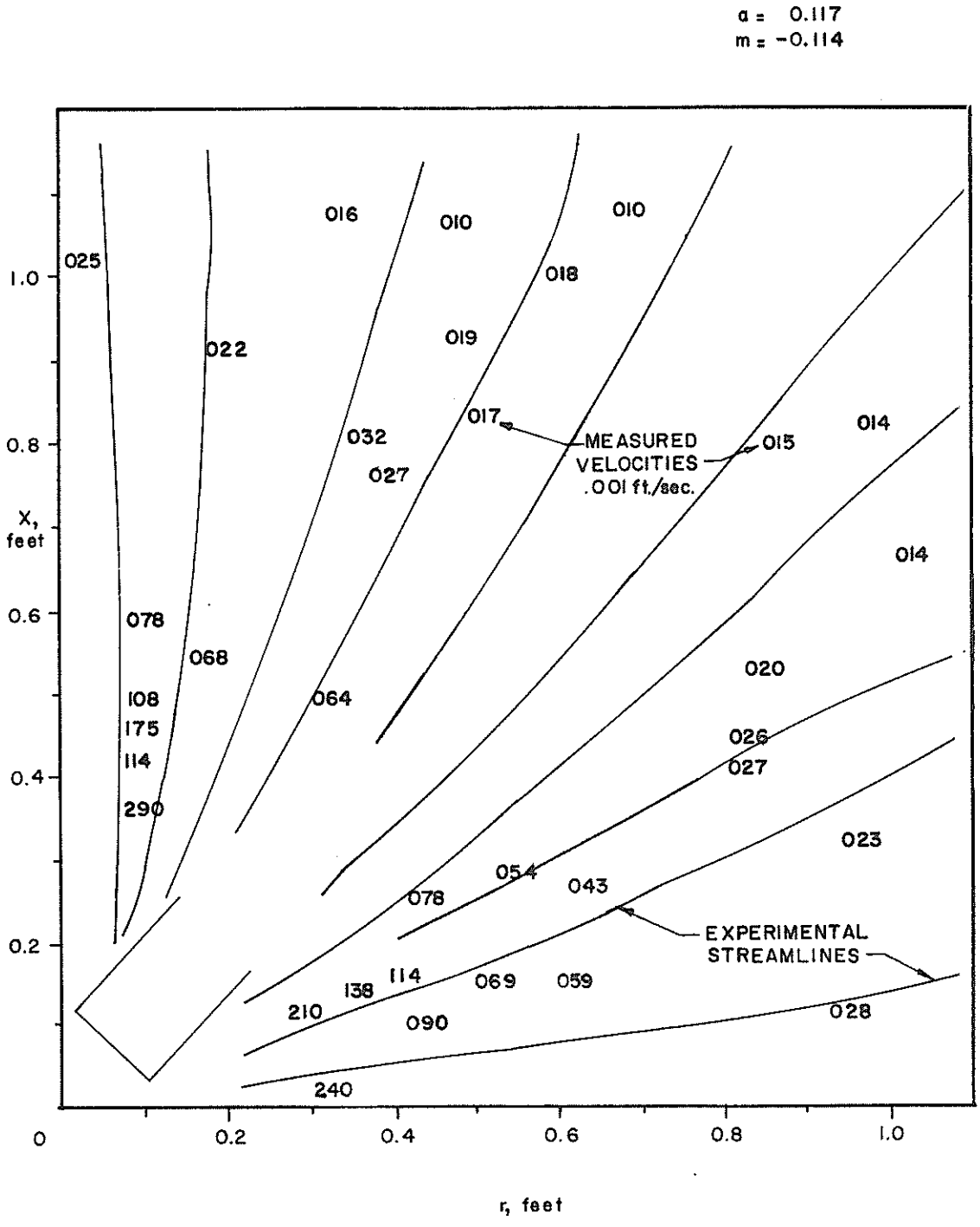

Fig. 18 Experimental Sink Flow, Rear, θ = 45°, a/D = 1.0, Q = 67 GPM

Experimental results of the nine flow cases are shown in Figs. 10 through 18. These nine cases are grouped together here to illustrate the type of data obtained. A quick inspection reveals that the stream lines progress smoothly toward the inlet and in general the velocities increase as they approach the inlet. The discrepancies in velocities illustrate two facts. Each of these figures is a composite of at least six test runs, and the actual flow conditions within a small area can be arbitrary due to local turbulence and transient conditions. The data shown here was taken within the first few minutes of each test run because of flow instabilities which will be discussed later.

The nine experimental flow cases were combined with the theoretical results in Figs. 19 through 27. A change has been made in the presentation of the theoretical data. The velocity potential lines are absent and the more meaningful lines of equal velocity are shown. These lines curve in more abruptly than velocity potential lines as they approach the bottom and they are not orthogonal to the stream lines. Also, note that the experimental streak lines in general agree quite well with the theoretical stream lines. Fig. 28 illustrates in dimensionless terms the rapid decrease in theoretical velocity with distance from the inlet, a) along the bottom and b) along a 45° angle from the center of the inlet.

Figs. 25, 26 and 27 show the flow fields on three sides of an inlet pipe at 45° to the vertical compared to the theoretical flow field. A careful examination of these figures indicates that with

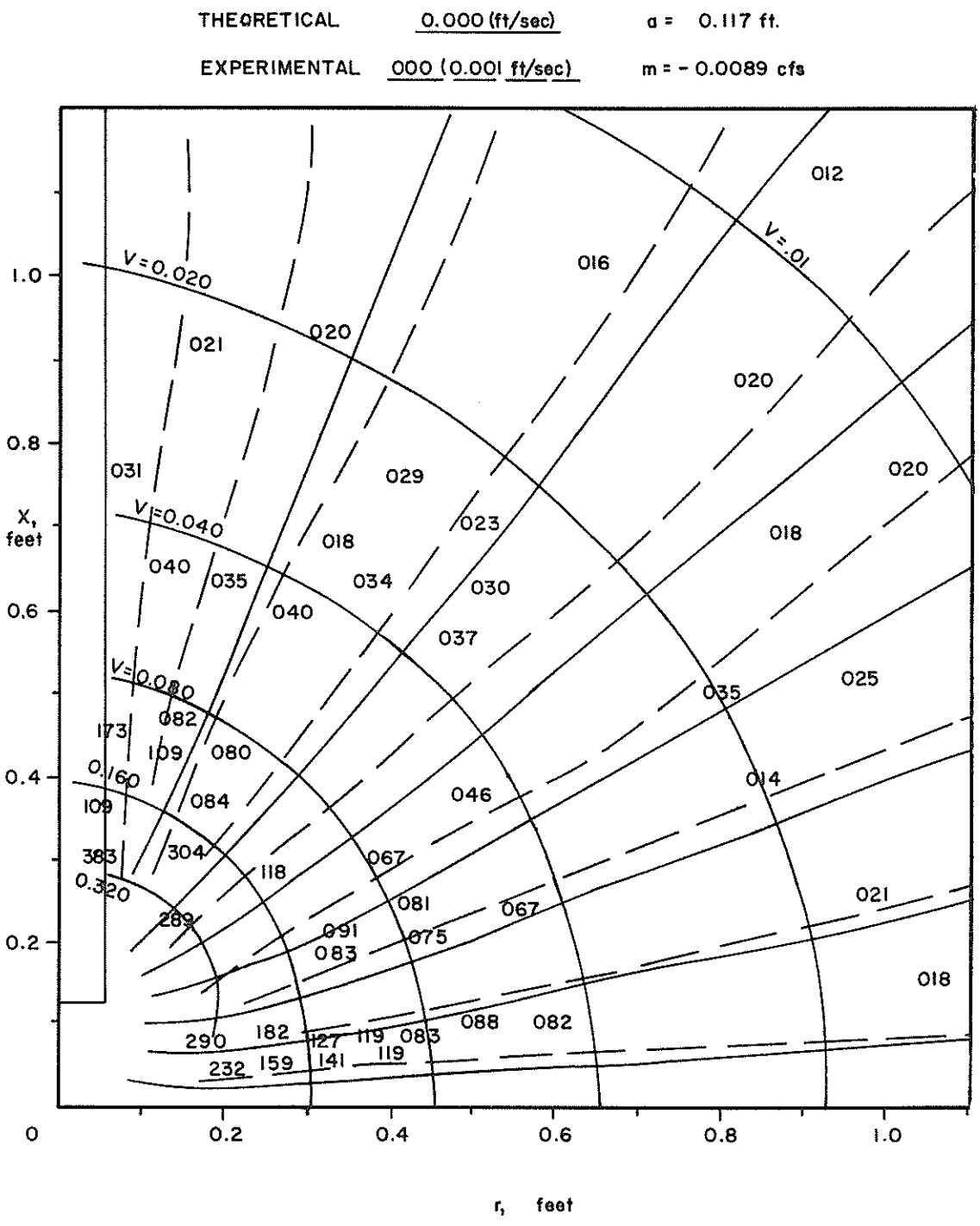

Fig. 19 Theoretical and Experimental Sink Flow, a/D = 1.0, Q = 50 GPM

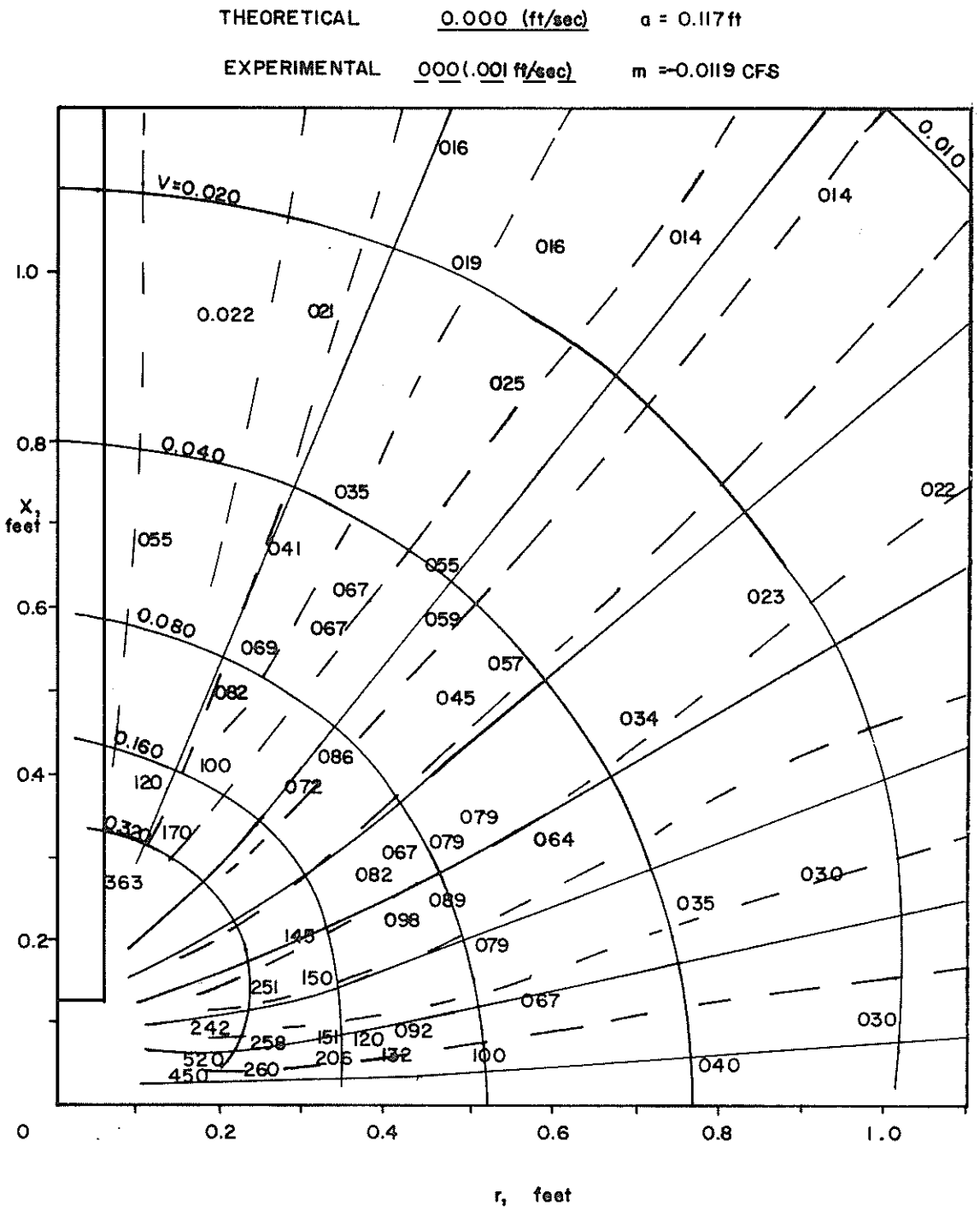

Fig. 20 Theoretical and Experimental Sink Flow, a/D = 1.0, Q = 67 GPM

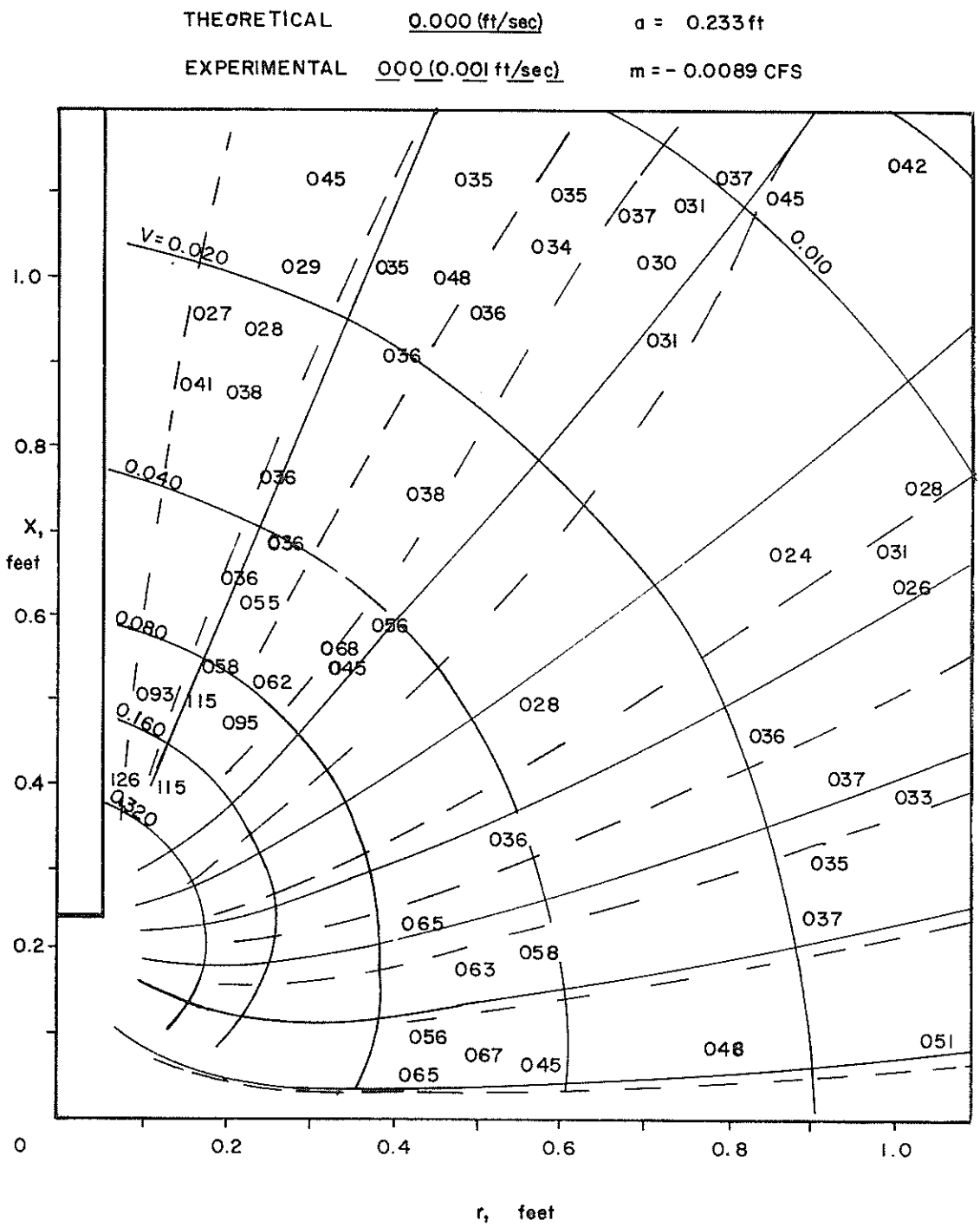

Fig. 21 Theoretical and Experimental Sink Flow, a/D = 2.0, Q = 50 GPM

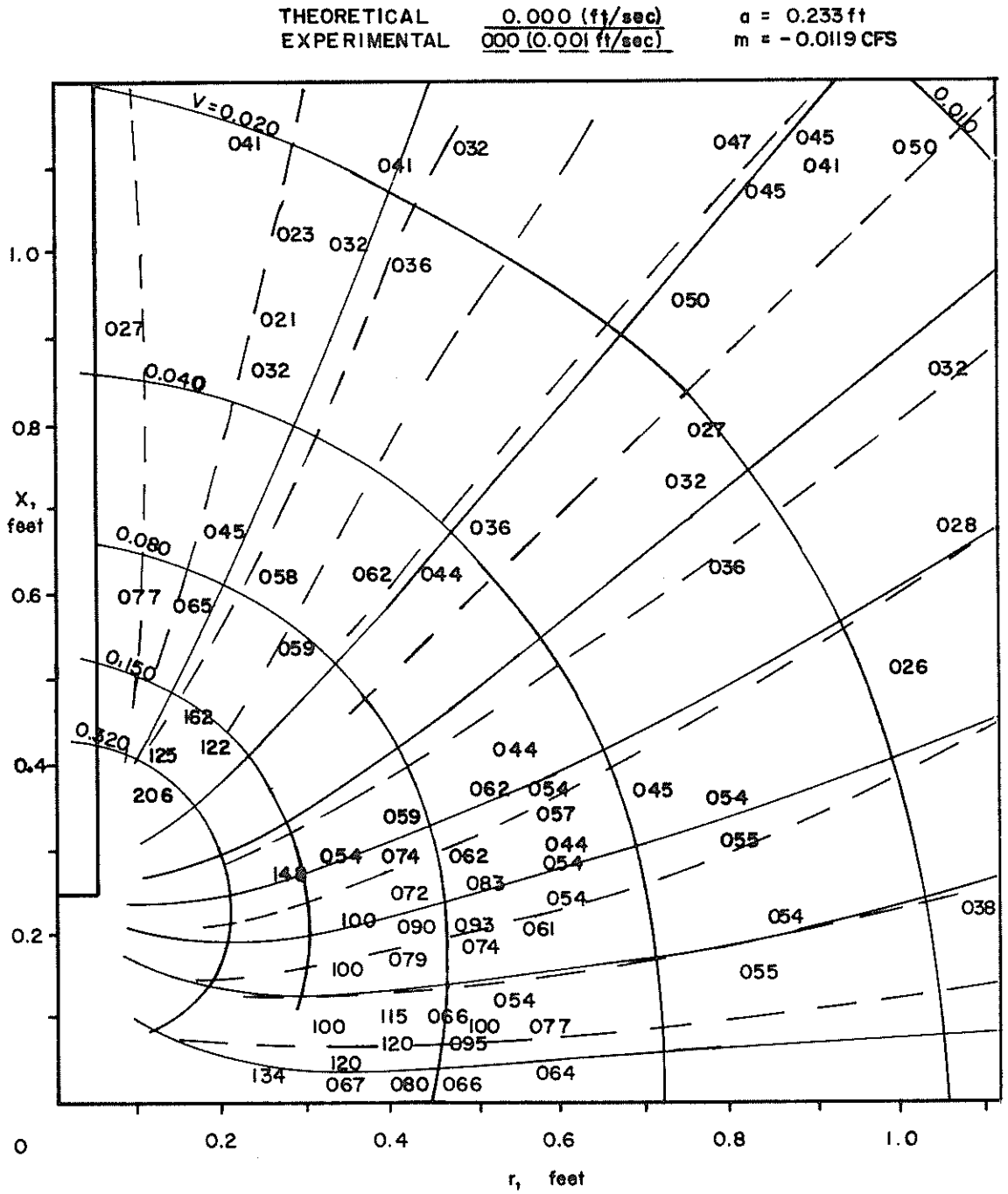

Fig. 22 Theoretical and Experimental Sink Flow, a/D = 2.0, Q = 67 GPM

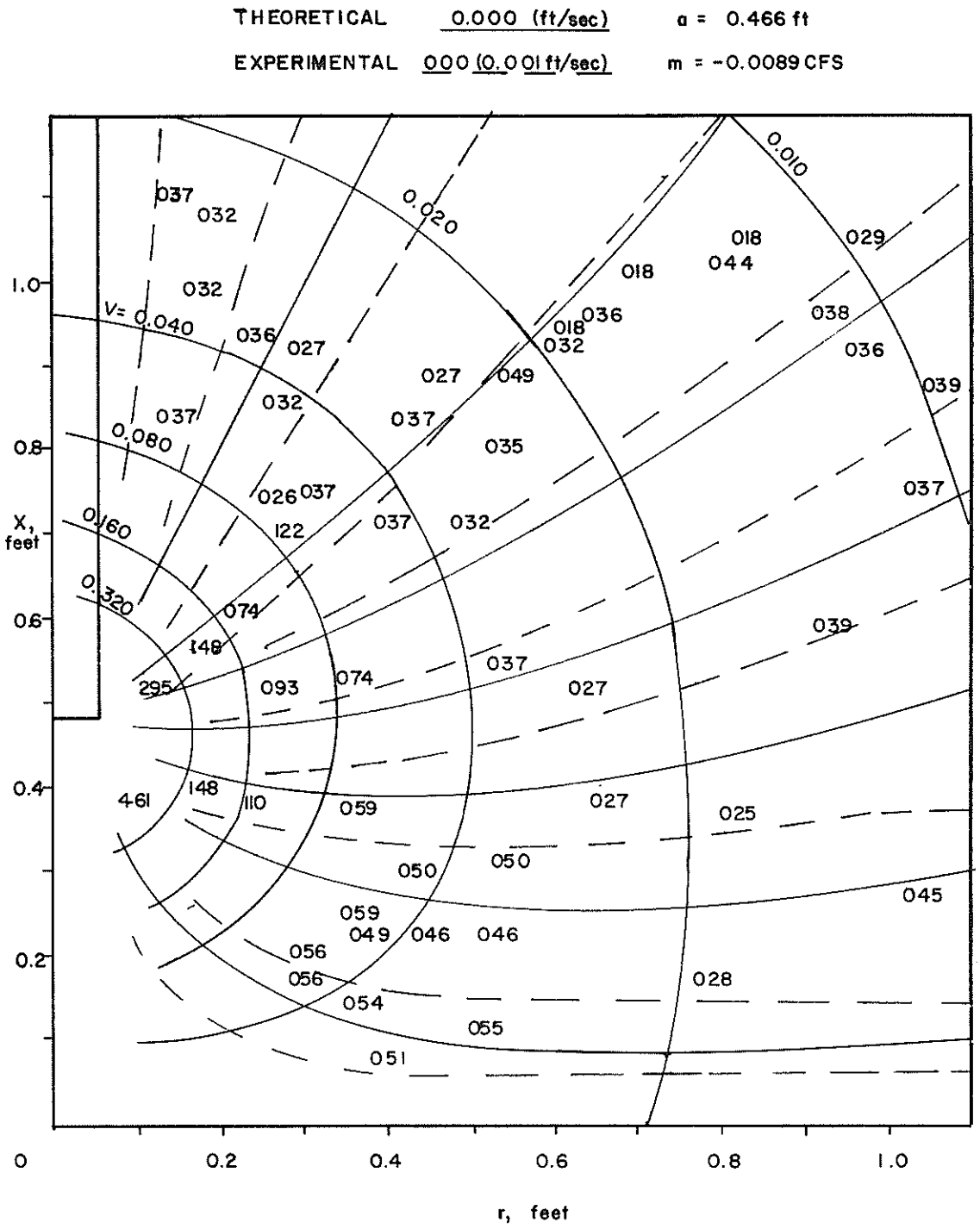

Fig. 23 Theoretical and Experimental Sink Flow, a/D = 4.0, Q = 50 GPM

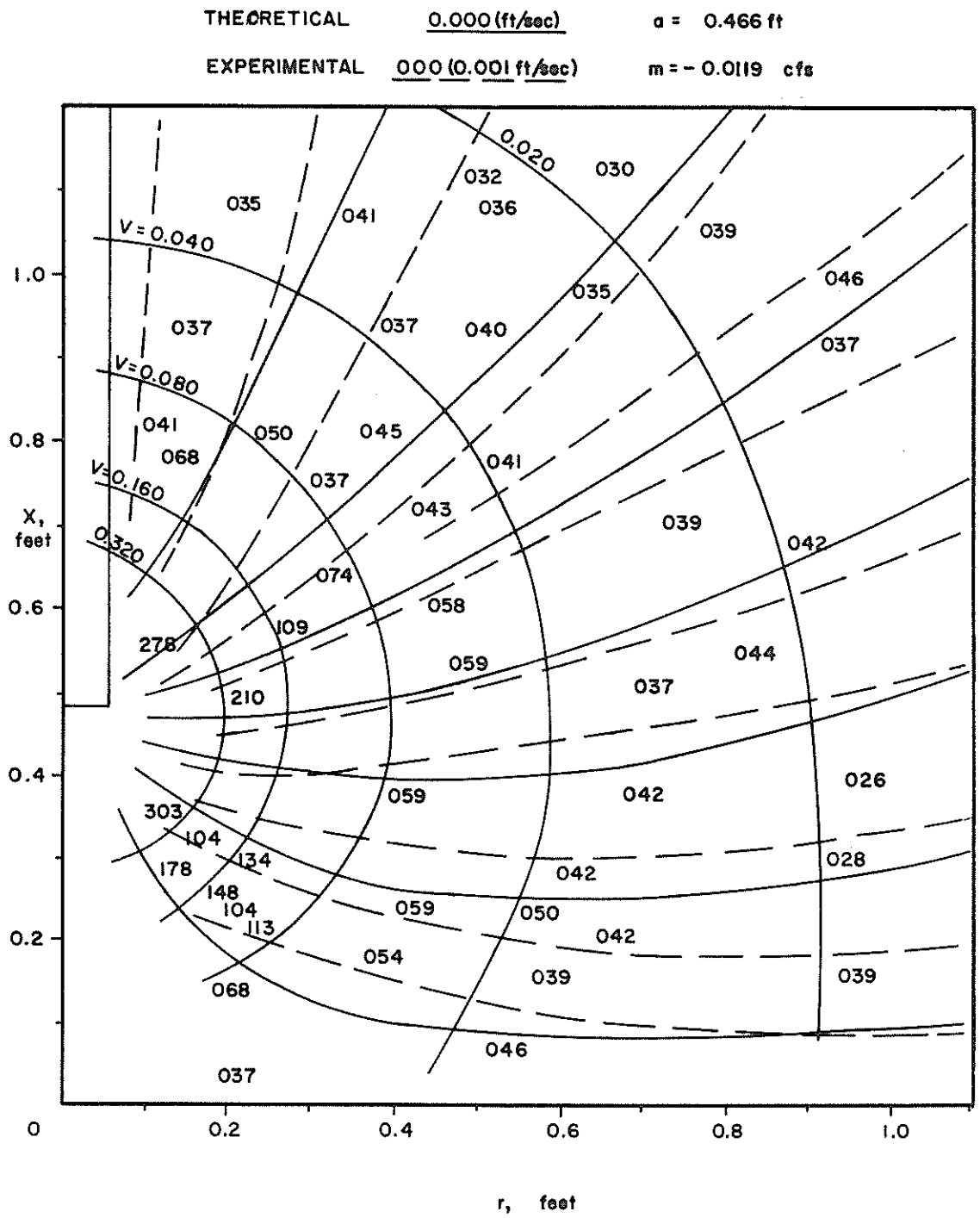

Fig. 24 Theoretical and Experimental Sink Flow, a/D = 4.0, Q = 67 GPM

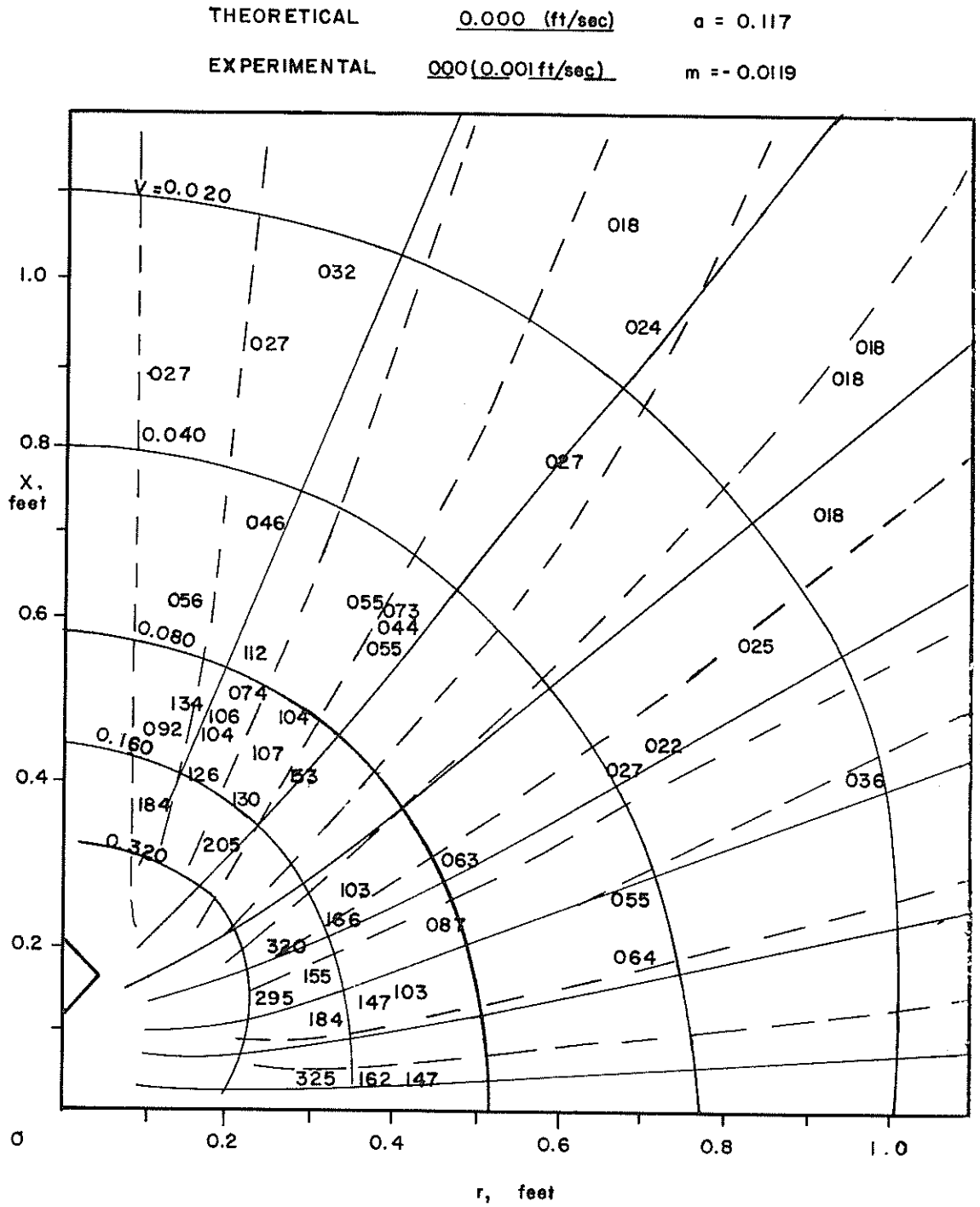

Fig. 25 Theoretical and Experimental Sink Flow, Front, $\theta = 45°$, A/D = 1.0, Q = 67 GPM

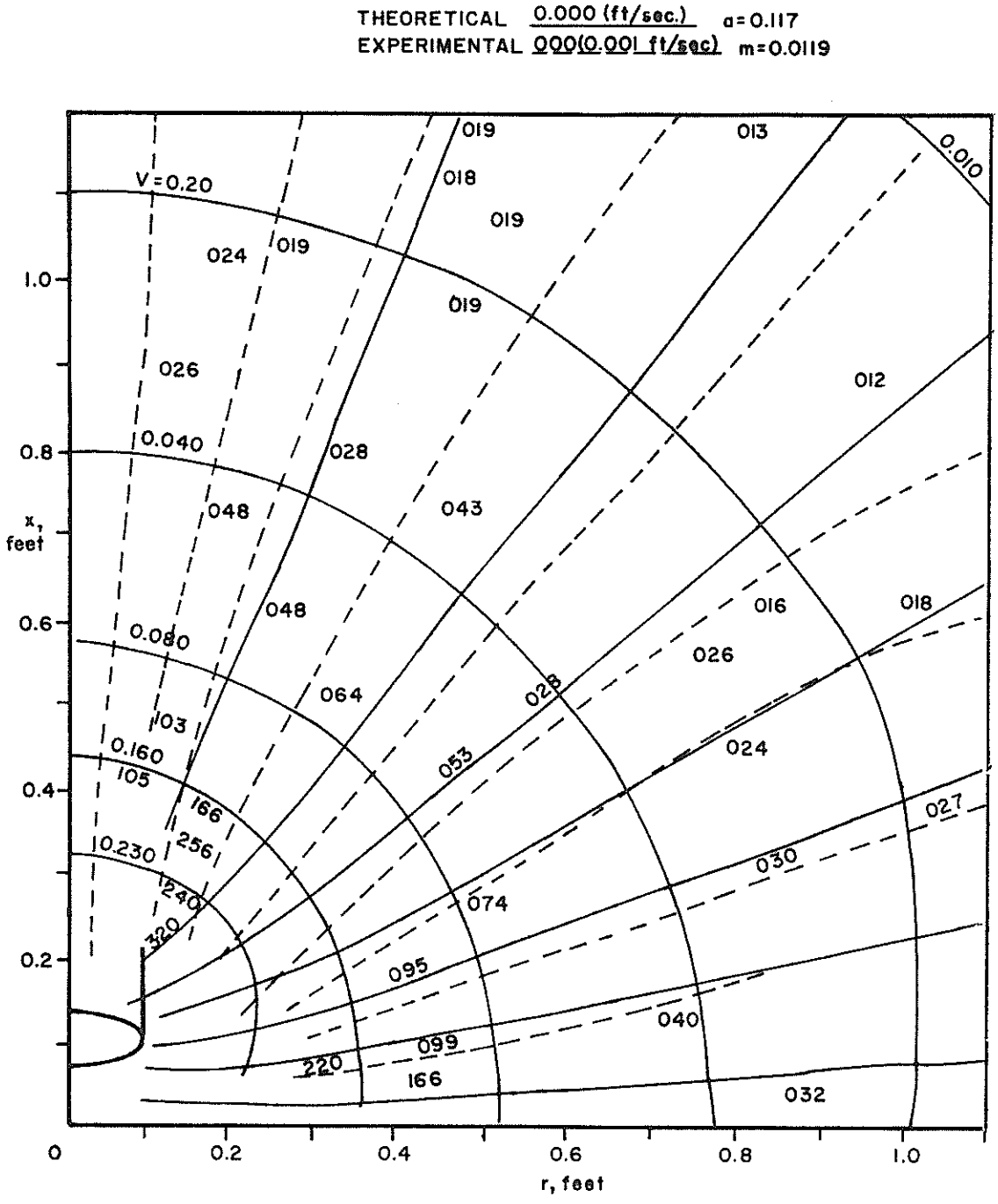

Fig. 26 Theoretical and Experimental Sink Flow, Side, $\theta = 45°$, $a/D = 1.0$, $Q = 67$ GPM

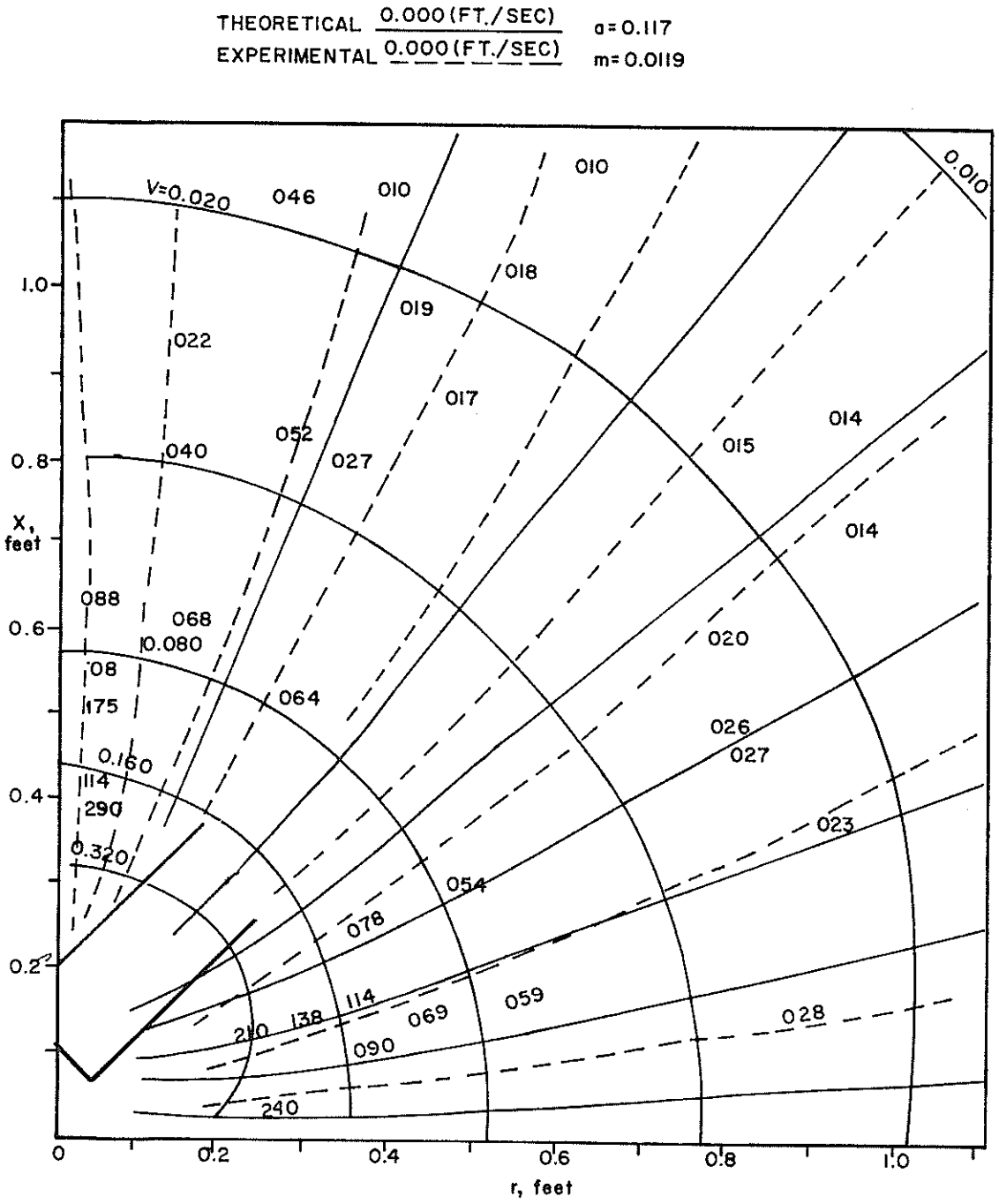

Fig. 27 Theoretical and Experimental Sink Flow, Rear, $\theta = 45°$, $a/D = 1.0$, $Q = 67$ GPM

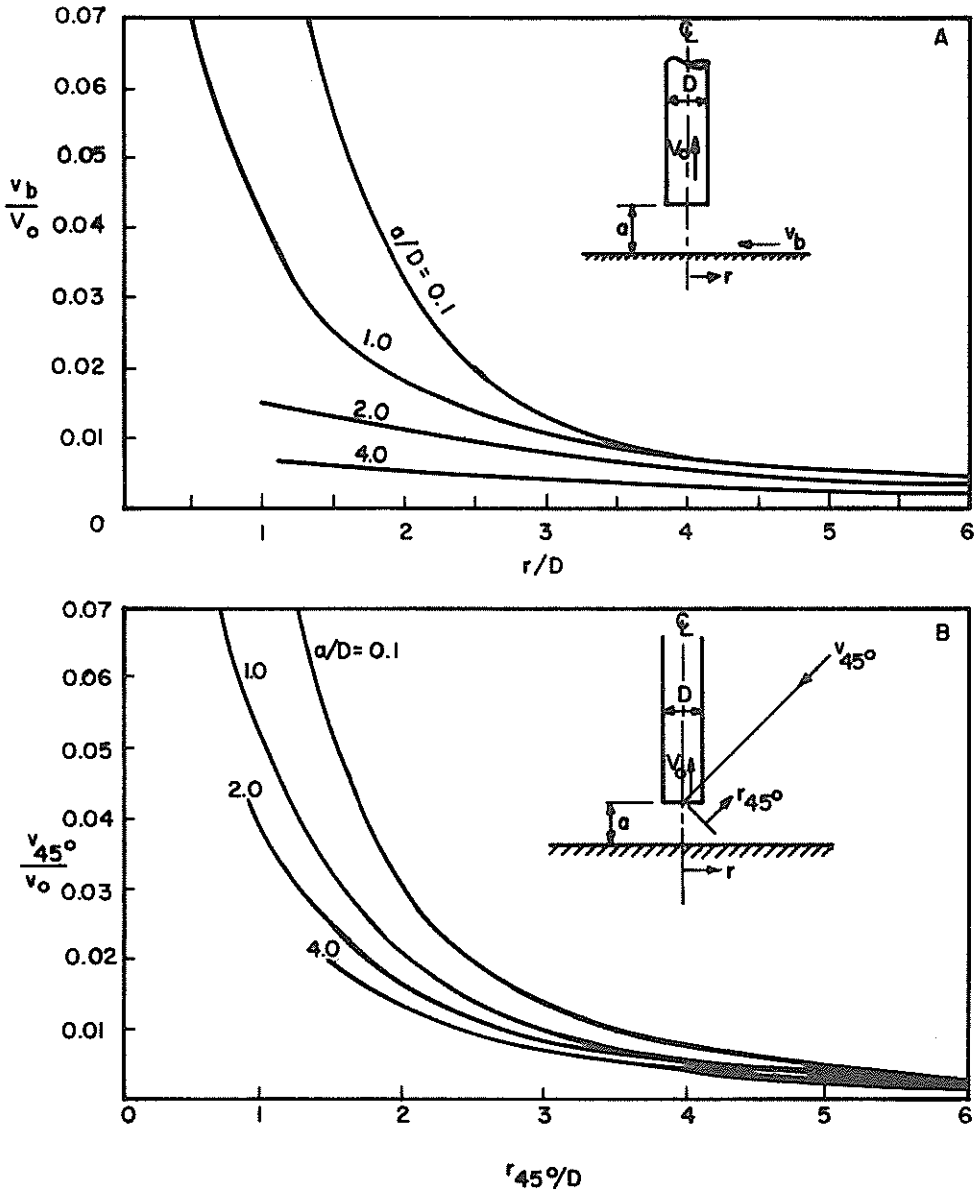

Fig. 28 Variation of Theoretical Velocity with Distance From Inlet

one exception most of the velocity values are close to the theoretical values. The exception is in Fig. 25. Several velocity values in front of the inlet and near the bottom are significantly high. This indicates that velocities near the bottom in front of an angled inlet pipe are significantly higher than equivalent positions beside and behind the inlet with other areas relatively unaffected by the inlet angle. However, this one case does not constitute an exhaustive study and this conclusion can be evaluated in that light.

A careful examination of Figs. 19 through 27 will show that something interesting and unanticipated is happening. In the five figures where a/D = 1.0 (Figs. 19, 20, 25, 26 and 27), most of the velocity values throughout the flow field agree, within acceptable limits, with the theoretical values. Now, observing the four figures where a/D = 2.0 and a/D = 4.0 (Figs. 21, 22, 23 and 24), note that the area away from the inlet past the line, V = 0.020 ft./sec., there are a large number of velocity values that are significantly higher than predicted by potential flow theory. At first, experimental error might be suspected except that this phenomenon occurs consistently in the four cases. Also, this situation helps explain the further development of the flow which will now be described.

As the time period for each experimental run progressed, the flow situation gradually changed. The streak lines would be displaced from their initial positions and the values for velocities changed. This change is illustrated by Fig. 29. Frame A shows the position of the initial streak lines. Frames B through E show how the streak

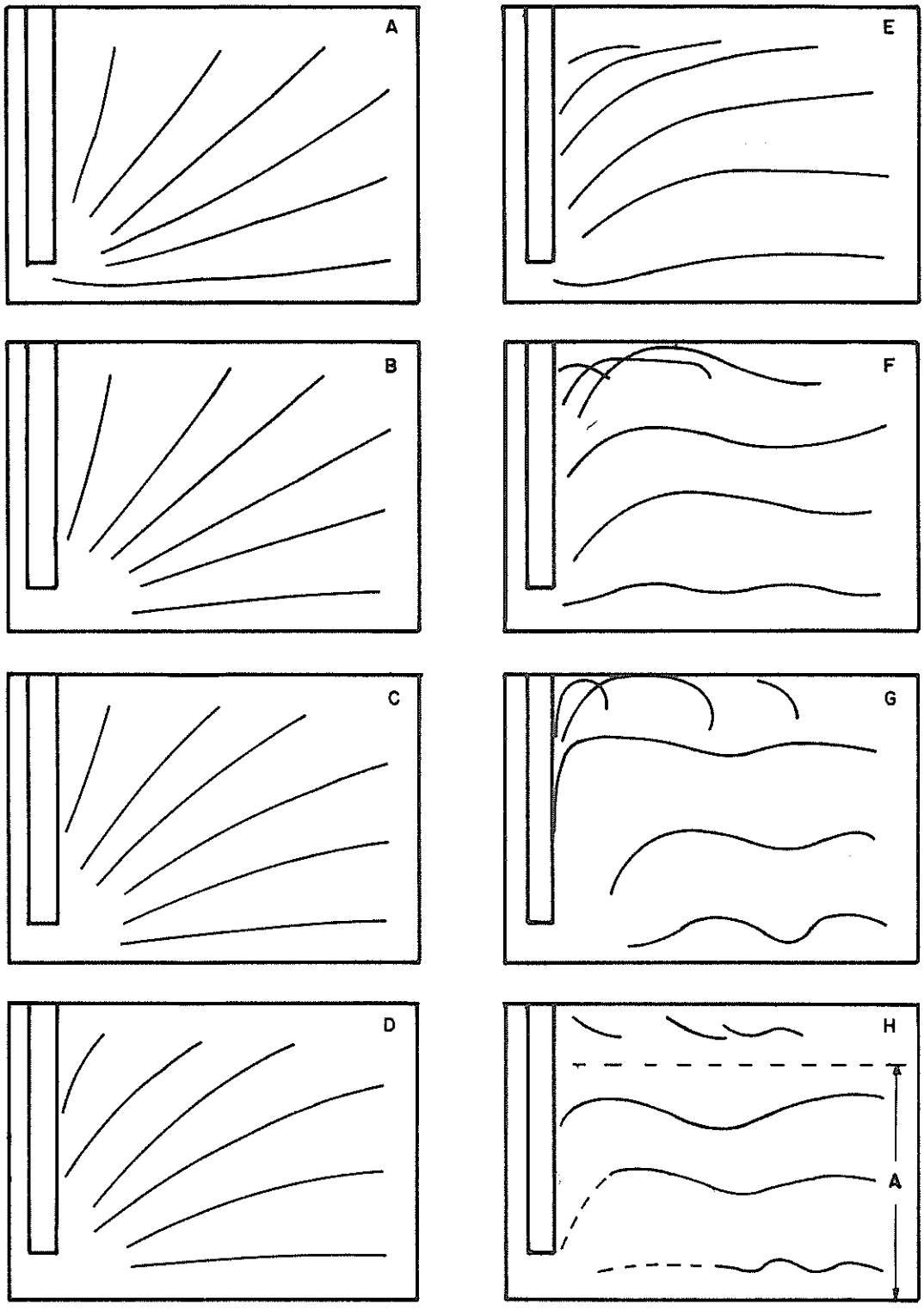

Fig. 29 Development of Flow

lines tend to become more horizontal away from the inlet. The velocities above the inlet decrease until (Frame F) reversal takes place. Velocities near the bottom increase. As the run continues, the flow becomes more unstable and the streak lines start to wave (Frame F) until general turbulence sets in and the dye streaks become difficult to observe (Frame G). This phenomenon occurs for both flow rates and all inlet positions. Instability does occur sooner for the higher flow rate. Fig. 30 shows an example of the change in velocity near the bottom during one test run.

The final flow configuration can be described qualitatively (Fig. 31). Streak lines tend to align themselves parallel to the bottom as they approach the inlet. Near the inlet the flow is similar to the theoretical in appearance but with higher velocities near the bottom. Above the inlet the flow becomes weak. Streak lines become wavy and intermittent flow reversal takes place. Above this area upward vertical flow takes place.

The flow just described can be explained by considering the forces involved and effects of the experimental apparatus itself. Initially, when the pump was switched on, a low pressure area was created at the mouth of the inlet pipe. A visible surge was observed throughout the tank as the fluid was accelerated. The initial flow configuration appeared to be the result of pressure and inertial forces almost exclusively as it agreed quite well with potential flow theory. As the flow developed, evidently other factors, such as boundary or viscous effects, became significant. Viscous forces make

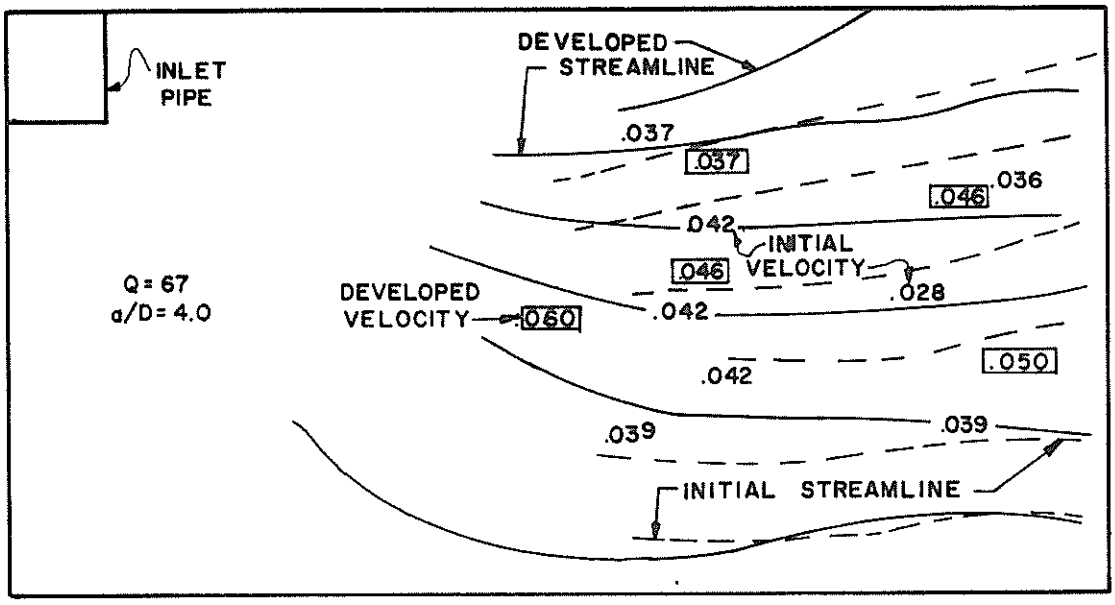

Fig. 30 Velocity Change Near Bottom

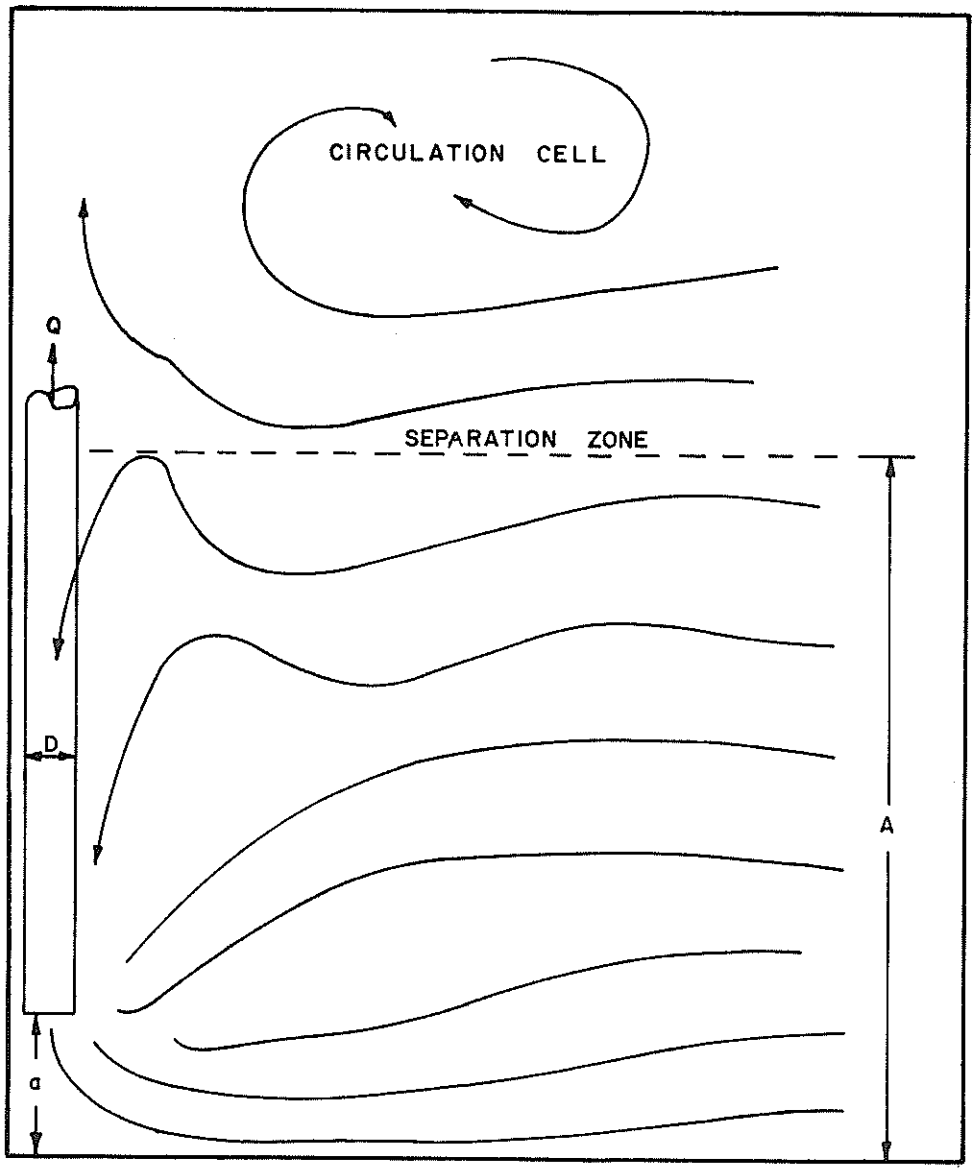

Fig. 31 Final Flow Configuration

a fluid tend to resist deformation. If viscous drag along the bottom is significant, then a lowering of velocities near the bottom would be expected. This is opposite to what was observed. Looking at a small volume of fluid may explain the observation. As the small volume of fluid approaches the inlet, it deforms in three planes. In potential flow theory, stretching occurs in one plane and convergence occurs in two planes (Fig. 32a). If viscous effects were to resist the convergence in one plane, then a flow resembling Fig. 32b may result. This resembles experimental observation. Viscous effects also explain the carrying along of fluid which is caught at the apex of the wedge above the inlet of Fig. 32 and displaced upward.

There should always be concern as to how the operation of the experimental apparatus itself affected results. The experimental tank was filled and performance tests run several times. After the tank had become still, crystals of potassium permanganate were dropped at intervals along the surface. As the crystals fell, they left a trail of deep purple coloration. As the pump was started, a detectable surge toward the inlet was observable in most areas of the tank. A situation which would have affected results would have been large scale circulation within the test section of the tank. Two types of circulation were observed. A weak intermittent cell of circulation developed in a vertical plane above and to the side of the inlet. This appeared to be a part of the flow development and not a result of tank geometry as the flow near the return flow filters was not

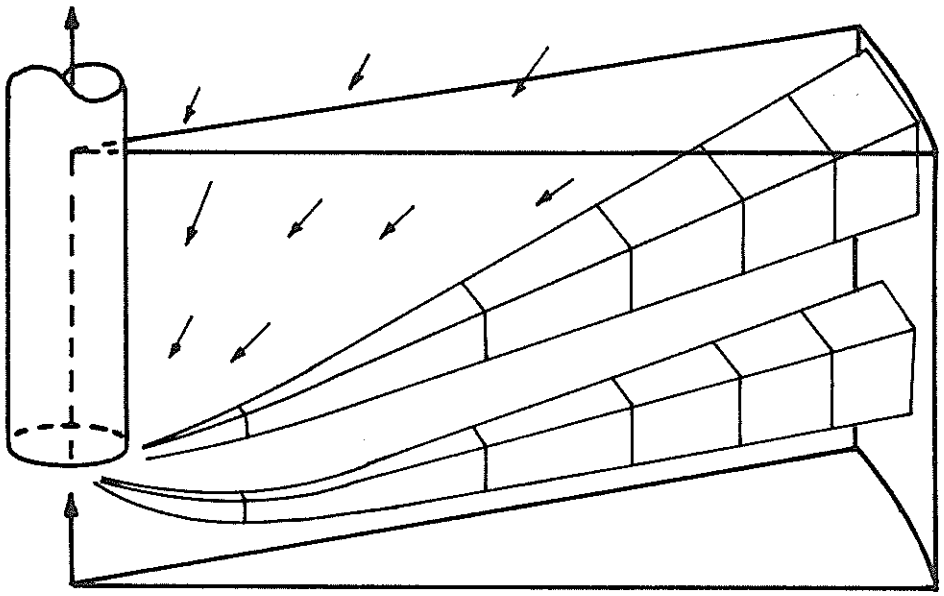

a. INITIAL

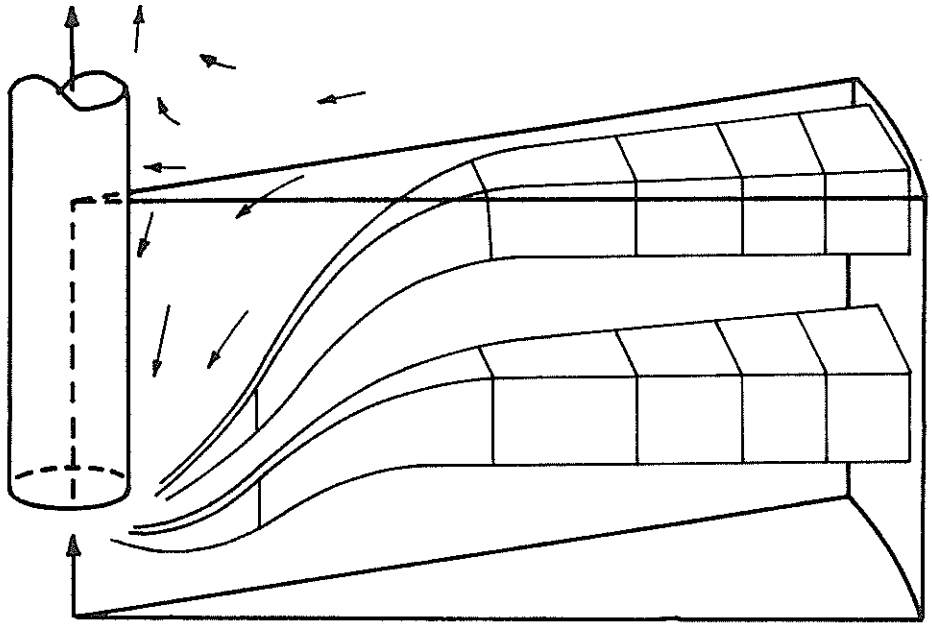

b. FINAL

Fig. 32 Possible Fluid Movement

dectectably affected. Another type of circulation was caused by uneven return flow. Uneven flow at the return filters constituted a small angular velocity in a horizontal plane relative to the inlet pipe. As this material approached the inlet, a significant angular velocity developed due to conservation of angular momentum. This problem was caused by improperly sealed return filters and was corrected by resealing these filters. As a result, this type of circulation was observed only after extended periods of pumping. Disturbances due to the return flow were small due to the very small and uniform return velocity over the entire return filter. However, it was suspected that some of the turbulence observed in the test section was transmitted through the return filters from the manifold area. Overall, the test facility was considered to be well suited to the scale used.

CONCLUSION

This study started with a straightforward theory which predicted the speed and direction of fluid particles in a fluid field around an inlet pipe near a flat boundary. Had the experimental results differed from the theory only slightly, then distortion factors would have been applied to improve the original equations. However, the results of this study are not improved equations. Insights have been gained into the functioning of this fluid phenomenon. This information should be particularly interesting to the hydraulic dredging field.

Some interesting information has been provided by this study. The theoretical equations presented can be used for a rough approximation for design purposes. However, for developed flow, zones of separation and zones of higher velocity were present. As the flow field developed, velocities and turbulence levels near the bottom increased. Both of these factors increase the sediment entrainment capacity of the flow. Angles of the inlet pipe of ninety and forty-five degrees to the horizontal did not produce significantly different flow fields. The ultimate experimental steady state flow development was difficult to identify due to the increasing presence of turbulence which caused the dye streak lines to fluctuate and mix with the fluid. In this developed flow, a horizontal zone of separation formed above the inlet. Velocities in this zone were low. Fluid below this zone was entrained in the inlet and fluid above the zone was deflected

upward. This latter effect could explain the tendency of turbid water to surface at a dredge site. The considerable scatter observed in experimental numbers was partially due to experimental techniques but mainly reflected the highly variable nature of the situation being studied.

Based on the limited results in this study and the finding of others the following conclusions are drawn:

1. A potential flow sink model of suction pipe flow near a boundary is impractical for describing the surrounding velocity field sometime after normal start-up conditions.
2. Viscous and boundary effects create separation zones and large scale circulation patterns which considerably alter the streamline patterns. These complexities need further study in order to take advantage of them in the design of more efficient and effective dredging intake systems.
3. The velocity decreases very rapidly with radius from the suction inlet in the theoretical model. This is true even when the pipe is a very small distance (a/D = 0.1) from the boundary. Although viscous effects alter the theoretical velocity-decrease curves presented, they are still of interest for real flows which undoubtly also exhibit a rapid drop in velocity in the surrounding velocity field.

RECOMMENDATIONS

Better information could be attained by an improved data taking and reduction system. The buoyant oil performed well but was difficult to see against a dark background. A light background, dark grid, and dark dye would help. A larger film size would also help data reduction. A projector that could automatically frame forward or backward a frame at a time would increase the speed and accuracy of data reduction. The flow rate and pipe size used were probably as large as was practical due to the level of disturbance they caused. A larger experiment could be assembled and lowered into Texas A&M University's largest flume where the return flow could be placed at a considerable distance from the observation window.

The results of this study are quite limited. A more thorough inspection of the photographic data could provide more quantitative information on the separation zone height, A, and velocities near the bottom. Further work needs to be done in these areas, especially for various inlet angles. Other factors that need to be considered are inlet size, inlet shape, water depth, and bottom slope. Time histories of bottom shear and turbulence levels could be measured with a hot film anemometer. In general, boundary effects, areas of separation, and areas of circulation need to be better understood in order to design more efficient and effective dredging intake systems. Actual models of dredge equipment incorporating new ideas could then be evaluated using techniques presented here or possibly

using model sediments.

There is a possible application of the information presented in this report to an existing dredge situation. The separation zone height, A, was observed to be roughly eight to ten diameters above the bottom. Placing a horizontal shield lower than this could artificially lower the zone of separation, increase velocities and turbulence near the bottom causing increased sediment entrainment, and could help prevent turbid water from reaching the surface. The shield should be shaped like an upright bowl so that it might be deflected by bottom irregularities and so that turbid water in its line of advancement might be deflected downward. The shield should not be placed so low that it significantly increases entrance losses. Such a device could improve both production and water quality. A schematic representation of a possible hooded cutterhead suction design is shown in Fig. 33.

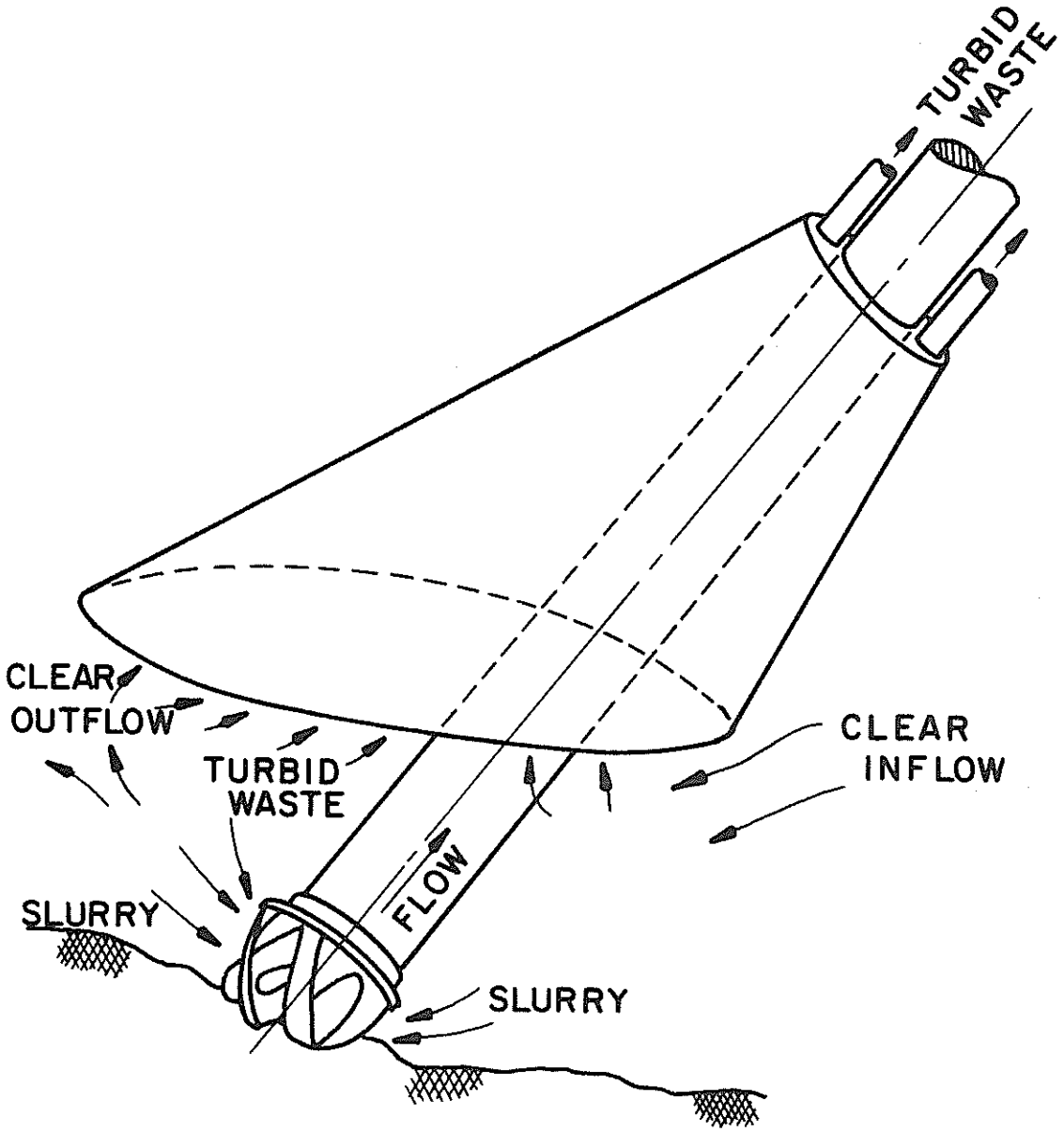

HOODED-CUTTERHEAD SUCTION

Fig. 33

APPENDIX I. - REFERENCES

1. A.S.M.E. Symposium, "Flow Visualization", 1960.

2. Clutter, D.W. and Smith, A.M.O., "Flow Visualization by Electrolysis of Water", Aerospace Engineering, January 1961, pp. 24-27 and 74-75.

3. DeKoning, J., "Field Observations of Density Flow to the Suction of a Suction Dredger in Sand Pits", Civil Engineering Public Works Review, Vol. 65, No. 765, April 1970, pp. 403-405.

4. Giesekus, V.H., "Nicht-lineare Effekte biem Stromen viskoelasticher Flussigkeiten durch Schiltz-und Lockdusen", Rheologica Acta, Band 7, Heft 2, 1968, pp. 127-138.

5. Holt, M., "Dimensional Analysis", Handbook of Fluid Dynamics (V.L. Streeter, ed.), McGraw-Hill, Inc., New York, 1961.

6. Marrucci, G., and Murch, R.E., "Steady Symmetric Sink Flows of Incompressible Simple Fluids", Industrial Engineering Fundamentals, Vol. 9, No. 3, 1970, pp. 498-500.

7. Metzner, A.B.; Uebler, E.A.; and Chan Man Fong, C.F., "Converging Flows of Viscoelastic Materials", American Institute of Chemical Engineers Journal, Volume 15, No. 5, September 1969, pp. 750-758.

8. Milne-Thomson, L.M., Theoretical Hydrodynamics, The MacMillan Co., New York, 1955.

9. Shames, I.H., Mechanics of Fluids, The McGraw-Hill, Inc., New York, 1962.

10. Slotta, L.S., "Flow Visualization Techniques Used in Dredge Cutterhead Evaluation", Proceedings of the World Dredging Conference, 1968, pp. 92-116.

11. Uebler, E.A., "Pipe Entrance Flow of Elastic Liquids", Ph.D. Dissertation, University of Delaware, June, 1966.

12. Valentine, H.R., Applied Hydromechanics, Plenum Press, Second Edition, Butterworth and Co., Ltd., London, 1967.

APPENDIX II. - NOTATION

The following symbols are used in this paper:

A = vertical distance from floor to horizontal plane of separation zone;

a = vertical distance from bottom to suction inlet;

D = inside diameter of inlet pipe;

h = manometer reading, inches of mercury;

L = an unspecified length term;

m = strength of source or sink;

N_r = Reynolds number;

Q = volumetric flow rate;

r = horizontal radius out from axis of symmetry;

r_{45} = distance from center of inlet on 45° angle;

V = velocity at a point;

V_b = velocity at a point on bottom;

V_o = average velocity in suction pipe;

V_r = r - component of velocity at a point;

V_x = x - component of velocity at a point;

$V_{45°}$ = velocity at a point on 45° axis;

x = vertical distance from floor;

ψ = stream function;

ϕ = velocity potential function;

θ = pipe angle from horizontal;

ρ = fluid density; and

μ = fluid viscosity.

APPENDIX III. - COMPUTER PROGRAMS

```
      //$WATFIV  JOB (321T2,C4-F-,*3,3C1,--),*  APGAR,  JACK      *       *   JOB 140
      C
      C ***************************************************************************
      C ***************************************************************************
      C
      C
      C                              POTENTIAL THEORY
      C
      C                          FLOW TO SINK NEAR BOUNDARY
      C
      C
      C ***************************************************************************
      C ***************************************************************************
      C
      C                                                    PROGRAMMED BY MARK B. PUCKETT
      C
      C A = DISTANCE OF SINK FROM BOUNDARY (FT)
      C M = STRENGTH OF SINK (CFS) = Q*(1/449)*(1/(4*PI)),  Q  IN GPM
      C XMAX & RMAX ARE THE MAXIMUM DISTANCES TO BE CONSIDERED ALONG THE AXES
      C DELTAX & DELTAR REPRESENT THE INCREMENTAL STEP SIZE ALONG THE AXES
      C PHI-LINES REPRESENT VELOCITY POTENTIAL LINES
      C PSI-LINES REPRESENT FLOW LINES
      C X & R VALUES ARE THE COORDINATES OF A POINT ON A PARTICULAR PHI- OR PSI-LINE
      C
    1         REAL M
    2         READ 111,A,Q,XMAX,RMAX,DELTAX,DELTAR
    3       111 FORMAT(6F10.3)
    4         M=Q/5642.
      C
      C ******************CALCULATING VARIOUS PHI-LINE COORDINATES*******************
      C
    5         PRINT 22,A,Q,M
    6        22 FORMAT('1',6X,'DATA'//10X,'A =',F6.3,' FT'//10X,'Q =',F6.1,' GPM'/
             C/10X,'M =',F7.4,' CFS'///24X,'PHI-LINE COORDINATES'///16X,'PHI',15
             CX,'X',15X,'R',35X,'NO. OF ITERATIONS')
      C ESTABLISHING MAXIMUM VALUE OF PHI, AND DIVIDING IT INTO INCREMENTS (DELPHI)
      C M  IS MULTIPLIED BY A SELECTED FACTOR WHICH CONTROLS THE SPACING AND
      C RELATIVE POSITION OF THE PHI-LINES
    7         PHIMAX=-6.*M
    8         DELPHI=PHIMAX/14.
      C ASSIGNING THE INITIAL VALUE OF PHI
    9         PHI=DELPHI
   10       4 PRINT 33,PHI
   11      33 FORMAT('0',11X,F8.4)
      C ASSIGNING A  X  VALUE AND ITERATING TO FIND THE CORESSPONDING  R  VALUE
   12         X=0.
   13       3 R=DELTAR
      C A MAXIMUM OF 200 ITERATIONS IS ALLOWED.  IF DESIRED ACCURACY IS NOT REACHED
      C THE CURRENT VALUES ARE PRINTED AND THE PROGRAM SKIPS TO THE NEXT POINT
   14         DO 1 I=1,200
   15         RNEW=-M*(R/PHI)*((((X-A)**2+R**2)**(-0.5))+(((X+A)**2+R**2)**(-0.5
             C)))
      C ACCUPACY CHECK
   16         IF(ABS(R-RNEW).LE.0.0001)GOTO2
   17         R=RNEW
   18       1 CONTINUE
      C PRINTING THE COORDINATES OF THE PHI-LINES
   19       2 PRINT 44,X,RNEW,I
   20      44 FORMAT(' ',29X,F8.3,8X,F8.3,40X,I3)
   21         IF(RNEW.GT.RMAX)GOTO9
```

```
      C INCREMENTING  X
   22         X=X+DELTAX
   23         IF(X.LE.XMAX)GOTO3
      C SOLVING THE SPECIAL CASE FOR  R = 0
   24         RADCAL=((4.*M**2)+(4.*(PHI**2)*(A**2)))**0.5
   25         X1=((-2.*M)+RADCAL)/(2.*PHI)
   26         X2=((-2.*M)-RADCAL)/(2.*PHI)
   27         PRINT 99,X1,X2
   28      99 FORMAT(' ',25X,'SPECIAL CASE FOR R = 0, X =',F8.3/53X,F8.3)
      C INCREMENTING  PHI
   29       9 PHI=PHI+DELPHI
   30         IF(PHI.LE.PHIMAX)GOTO4
      C ***************************************************************************
      C
      C ******************CALCULATING VARIOUS PSI-LINE COORDINATES******************
      C
   31         PRINT 55
   32      55 FORMAT('1',23X,'PSI-LINE COORDINATES'///16X,'PSI',15X,'X',15X,'R',
             C35X,'NO. OF ITERATIONS')
      C ESTABLISHING MAXIMUM VALUE OF PSI, AND DIVIDING IT INTO INCREMENTS (DELPSI)
      C M  IS MULTIPLIED BY A SELECTED FACTOR WHICH CONTROLS THE SPACING AND
      C RELATIVE POSITION OF THE PSI-LINES
   33         PSIMAX=-2.0*M
   34         DELPSI=PSIMAX/14.
      C ASSIGNING THE INITIAL VALUE OF PSI
   35         PSI=DELPSI
   36       8 PRINT 33,PSI
      C ASSIGNING A  'R'  VALUE AND ITERATING TO FIND THE CORESSPONDING  'X'  VALUE
   37         R=DELTAR
   38       7 X=DELTAX
      C A MAXIMUM OF 200 ITERATIONS IS ALLOWED.  IF DESIRED ACCURACY IS NOT REACHED
      C THE CURRENT VALUES ARE PRINTED AND THE PROGRAM SKIPS TO THE NEXT POINT
   39         DO 5 I=1,200
   40         XNEW=A-(PSI/M)*(((X-A)**2+R**2)**0.5)-(X+A)*(((X-A)**2+R**2)**0.5)
             C/(((X+A)**2+R**2)**0.5)
      C ACCURACY CHECK
   41         IF(ABS(X-XNEW).LE.0.0001)GOTO6
   42         X=XNEW
   43       5 CONTINUE
      C PRINTING THE COORDINATES OF THE PSI-LINES
   44       6 PRINT 66,XNEW,R,I
   45      66 FORMAT(' ',28X,F8.3,8X,F8.3,40X,I3)
   46         IF(XNEW.GT.XMAX)GOTO10
      C INCREMENTING  R
   47         R=R+DELTAR
   48         IF(R.LE.RMAX)GOTO7
      C INCREMENTING  PSI
   49      1( PSI=PSI+DELPSI
   50         IF(PSI.LE.PSIMAX)GOTO8
      C ***************************************************************************
   51         PRINT 77
   52      77 FORMAT('1')
   53         STOP
   54         END

      //$DATA
```

VEL0C2 06/05/73

```
30C  EQUAL VELOCITY LINES FOR POINT SINK NEAR A SOLID BOUNDARY.
40C
50C          PROGRAMMED BY JACK APGAR 6/1/73
60C
70C
100 DIMENSION V(7),M(2),A(6)
110 REAL M
111 ZERO=0.0
120 A(1)=.0
130 A(2)=.0117
140 A(3)=.0585
150 A(4)=.117
160 A(5)=.223
170 A(6)=.466
180 M(1)=-.0089
190 M(2)=-.0119
200 V(1)=.01
210  DO 3 K=2,7
220 3 V(K)=2*V(K-1)
230 DO25 I=1,6
240 DO25 J=1,2
250 PRINT 15,A(I),M(J)
260 15 FORMAT(" "//5X,"A=",F7.4/5X,"M=",F7.4//3X,"R",5X,"X",5X,
270&"V",6X,"VR",5X,"VX",3X,"VCHK",2X," ITERATIONS"//)
280 DO25 K=1,7
290 PRINT 16
300 X=A(I)+.1
310 DO 66 N=1,300
330 X=X*1.01
340 VX=M(J)*((X-A(I))**(-2)+(X+A(I))**(-2))
350 IF((V(K)+VX).GE.0.0)GOTO67
360 66 CONTINUE
361 67 VCHK=ABS(VX)
370 PRINT 22,ZERO,X,V(K),ZERO,VX,VCHK,N
380 DELX=X/9.0
385 XNEW=X
390 DO 24 L=1,8
400 R=.01
410 XNEW=XNEW-DELX
420 B=XNEW-A(I)
430 C=XNEW+A(I)
440 DO 17 N=1,200
450 D=(B**2+R**2)**1.5
460 E=(C**2+R**2)**1.5
470 VX=M(J)*(B/D+C/E)
480 VR=M(J)*R*(1.0/D+1.0/E)
490 VCHK=SQRT(VX**2+VR**2)
500 RNEW=R*VCHK/V(K)
510 IF(ABS(R-RNEW).LE..0001)GOTO 20
520 IF (ABS(RNEW).GT.5E5)GOTO24
```

VELOC2 06/05/73

```
530 R=RNEW
540 16 FORMAT(1H ,///)
550 17 CONTINUE
560 20 PRINT 22,RNEW,XNEW,V(K),VR,VX,VCHK,N
570 22 FORMAT(2X,F5.3,2F6.3,2F7.3,F6.3,I8)
580 24 CONTINUE
590 R=.01
600 DO 88 N=1,300
610 R=R*1.02
620 VR=2.*M(J)*R*((A(I)**2+R**2)**(-1.5))
630 IF(V(K)+VR.GT.0.0)GOTO 89
640 88 CONTINUE
650 89 VCHK=ABS(VR)
660 PRINT 22,R,ZERO,V(K),VR,ZERO,VCHK,N
680 25 CONTINUE
700 STOP;END
```